ARTICLE

doi:10.1038/nature14887

# The mechanism of DNA replication termination in vertebrates

James M. Dewar[1], Magda Budzowska[1] & Johannes C. Walter[1,2]

**Eukaryotic DNA replication terminates when replisomes from adjacent replication origins converge. Termination involves local completion of DNA synthesis, decatenation of daughter molecules and replisome disassembly. Termination has been difficult to study because termination events are generally asynchronous and sequence nonspecific. To overcome these challenges, we paused converging replisomes with a site-specific barrier in *Xenopus* egg extracts. Upon removal of the barrier, forks underwent synchronous and site-specific termination, allowing mechanistic dissection of this process. We show that DNA synthesis does not slow detectably as forks approach each other, and that leading strands pass each other unhindered before undergoing ligation to downstream lagging strands. Dissociation of the replicative CMG helicase (comprising CDC45, MCM2–7 and GINS) occurs only after the final ligation step, and is not required for completion of DNA synthesis, strongly suggesting that converging CMGs pass one another and dissociate from double-stranded DNA. This termination mechanism allows rapid completion of DNA synthesis while avoiding premature replisome disassembly.**

DNA replication occurs in three broad stages: initiation, elongation and termination. Termination occurs when converging replication forks meet and involves at least four processes, not necessarily in the following order. First, the last stretch of parental DNA between forks is unwound (dissolution) and replisomes come into contact; second, any remaining gaps in the daughter strands are filled in and nascent strands are ligated (ligation); third, double-stranded (ds)DNA intertwinings (that is, catenanes) are removed (decatenation); fourth, the replisome is disassembled. Despite decades of research on termination[1], we know little about the order, mechanism and regulation of the above events, especially during eukaryotic chromosomal replication.

Termination has been most extensively studied in the mammalian DNA tumour virus SV40 (ref. 2), where converging replication forks stall during termination[1,3,4]. Dissolution during SV40 replication requires rotation of the entire fork to produce catenations behind the fork (pre-catenanes)[5,6], which are resolved by topoisomerase (Topo) II (ref. 6), probably in a manner similar to how Topo IV functions during bacterial termination[7,8]. The SV40 replicative helicase, large T antigen, dissociates from chromatin before dissolution, but whether this is required for the completion of replication is unknown[9,10]. After dissolution, daughter strands retain gaps of ~60 nucleotides[11], which are ultimately filled in by an unknown mechanism in parallel to decatenation[12].

Eukaryotic termination has also been investigated. Although convergent forks accumulate at certain replication pause sites in yeast cells lacking 5′–3′ DNA helicases[13–15], it is unknown whether forks stall during unperturbed termination. Furthermore, Topo II is not required for dissolution in budding yeast[16,17] or during vertebrate termination[18,19]. Recent work shows that late in S phase, the eukaryotic replicative helicase CMG[20–23] is removed from chromatin by the ATPase p97 after ubiquitylation of MCM7 (by $SCF^{Dia2}$ in yeast)[24,25]. While one study implied that DNA replication can go to completion in the absence of CMG unloading[24], another reported that tracts of unreplicated DNA remain in the absence of this process[25]. Given that mis-regulation of bacterial termination can readily trigger re-replication of DNA[26,27], a potent driver of genomic instability in mammalian cells[28], a better understanding of eukaryotic termination is essential.

Owing to stochastic origin firing[29,30] and variable rates of replisome progression[31,32], the location and timing of eukaryotic termination is variable[30,33], making this process difficult to study. Here we report that *Xenopus* egg extracts can be used to induce synchronous and localized termination events. This approach has allowed us to identify and order key events underlying vertebrate termination.

## A system to study replication termination

Our strategy was to stall forks on either side of a reversible replication fork barrier (Fig. 1a, panels i–iii), and subsequently disassemble the barrier to trigger localized and synchronous termination events (Fig. 1a, panel iv). The barrier that we employed consisted of an array of *lac* repressors (LacRs) bound to *lac* operators (*lacO*s)[34,35], which can be disrupted by IPTG. We constructed p[$lacO_{16}$], which contains 16 tandem copies of *lacO* (490 base pairs (bp)). p[$lacO_{16}$] was incubated in nucleus-free *Xenopus* egg extract, which promotes sequence-nonspecific replication initiation on added DNA molecules, followed by a single, complete round of DNA synthesis via a mechanism that appears to reflect events in cells[36]. To monitor replication, radioactive [$\alpha$-$^{32}$P]dATP was included in the reaction. When p[$lacO_{16}$] was replicated in the absence of LacR for ~5 min and then cut with XmnI (Fig. 1a, panel iii), a single linear species representing fully replicated daughter molecules was observed (Fig. 1c, lane 1). In contrast, in the presence of LacR, a slow-mobility product appeared (Fig. 1c, lane 4) that corresponds to a double-Y structure, as shown by 2D gel electrophoresis (Extended Data Fig. 1a). To confirm that the double-Y resulted from fork stalling at the outer edges of the array, we separately monitored replication in the plasmid backbone and in the *lacO* array. In the presence of LacR, synthesis of the array was specifically delayed (Extended Data Fig. 1f). In contrast, LacR had no effect on replication of a plasmid lacking *lacO* sites (Extended Data Fig. 1e). These results indicate that replication forks stalled on both sides of the LacR array, consistent with previous findings[34,35,37].

[1]Department of Biological Chemistry and Molecular Pharmacology, Harvard Medical School, Boston, Massachusetts 02115, USA. [2]Howard Hughes Medical Institute, Department of Biological Chemistry and Molecular Pharmacology, Harvard Medical School, Boston, Massachusetts 02115, USA.

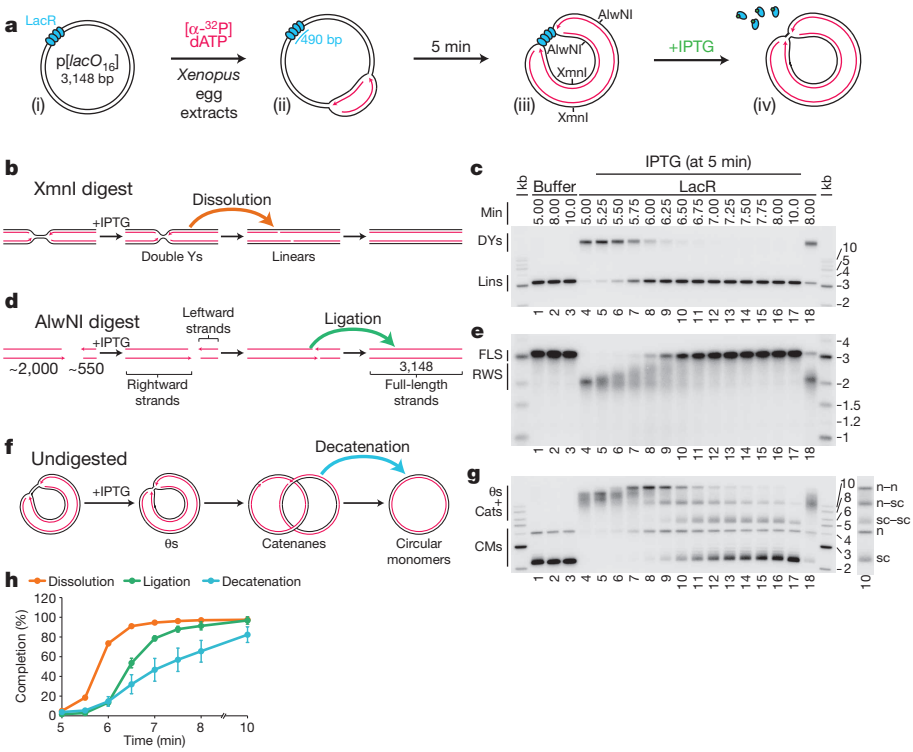


**Figure 1 | A model system to study replication termination.** **a**, Scheme to induce site-specific termination. Key restriction sites are highlighted. **b**, Schematic of the dissolution assay. **c**, p[$lacO_{16}$] was incubated in buffer or LacR, then replicated in the presence of [α-$^{32}$P]dATP, before termination was induced by the addition of IPTG. To measure dissolution, radiolabelled termination intermediates were cut with XmnI, separated on a native agarose gel, and analysed by autoradiography. **d**, Schematic of the ligation assay. **e**, To measure ligation, replication intermediates were cut with AlwNI and separated on a denaturing agarose gel. **f**, Schematic of the decatenation assay. **g**, To measure decatenation, replication intermediates were separated on a native agarose gel. The additional copy of lane 10 highlights catenated termination intermediates. Cats, catenanes; CMs, circular monomers; DYs, double-Y structures; FLS, full-length strands; Lins, linears; LWS, leftward strands; n–n, nicked–nicked; n–sc, nicked–supercoiled; RWS, rightward strands; sc–sc, supercoiled–supercoiled; kb, kilobase ladder, with the size of each band (in kilobases) labelled. **h**, Multiple dissolution, ligation and decatenation assays were quantified. Means ± standard deviation (s.d.) are plotted ($n = 4$).

We next addressed whether replication forks stalled by LacR could restart. When IPTG was added to double-Y structures 5 min after replication initiation, 90% were converted to unit-sized linear plasmid molecules within a further 1.5 min (Fig. 1c, lanes 5–10 and Fig. 1h, yellow circles). In the absence of IPTG, only 21% of double-Y molecules disappeared after 3 min (Fig. 1c, lane 18). The conversion of double-Y molecules to linear species occurs when any remaining parental DNA holding daughter molecules together is unwound (Fig. 1b). This process, which we refer to as 'dissolution', represents a convenient means to measure the point at which converging replisomes meet. Notably, the ATR–Chk1 pathway was not activated above background levels during this procedure (data not shown).

After dissolution, nascent strands should undergo ligation. To detect the growth and ligation of nascent strands, we digested p[$lacO_{16}$] with AlwNI, which cuts the plasmid once, ~550 nucleotides (nt) from the rightward edge of the array and ~2,000 nt from its leftward edge (Fig. 1a, panel iii, and Fig. 1d), and we analysed the products on a denaturing gel. Before IPTG addition, discrete species of ~2,000 nt (Fig. 1e, lane 4) and ~550 nt (Extended Data Fig. 2a, lane 4) were observed. Upon IPTG addition, both bands grew heterogeneously (Fig. 1e and Extended Data Fig. 2a). Since all leading strands were immediately extended upon IPTG addition (Extended Data Fig. 2b, c), we infer that the heterogeneity observed resulted because growth of the lagging strand was delayed until ligation of an additional Okazaki fragment. Finally, the nascent strands increased abruptly to the full length of 3,100 nt as ligation to downstream lagging strands occurred (Fig. 1e, lanes 9–13). As expected, dissolution preceded ligation, and there was an ~45 s delay between these two events (Fig. 1h).

Another important event associated with termination is decatenation of daughter molecules[18]. To measure this process, we analysed undigested replication products on native agarose gels (Fig. 1f, g). Before addition of IPTG, when the array had not yet been duplicated, replication products migrated as a compact smear of high-molecular-weight θ structures (Fig. 1f and Fig. 1g, lane 4). Upon addition of IPTG, most θ structures were lost within 1 min, and they were successively converted into three types of dimeric catenanes described previously[5,18,38]: nicked–nicked, nicked–supercoiled, and supercoiled–supercoiled (Fig. 1g and Extended Data Fig. 3a). Nicked–nicked catenanes appeared first (Fig. 1g, lanes 7, 8), followed by nicked–supercoiled (lanes 8–10) and supercoiled–supercoiled (Fig. 1g, lanes 9–12). Supercoiling is the result of nucleosome assembly on closed circular DNA[39]. Finally, monomeric, supercoiled daughter molecules accumulated (sc, Fig. 1g, lane 17) dependent on Topo II (Extended Data Fig. 3b–d) as seen *in vivo*[16,17]. Topo II was not required for dissolution or ligation (Extended Data Fig. 3c, d), suggesting that these processes proceed independently of decatenation[16,17,19]. Like ligation, decatenation began ~40 s after dissolution, but progressed at a slower rate than ligation (Fig. 1h). The same intermediates were detected in the absence of LacR, but their order of appearance was not well defined (Extended Data Fig. 3e).

Our results demonstrate that a reversible replication fork barrier allows induction of a synchronous and spatially defined termination event. They also show that soon after forks meet, as measured by dissolution, daughter molecules are quickly ligated and decatenated.

## Converging replication forks do not stall

To test the proposal that replication forks slow down or stall during termination[1,3,4], we quantified the rate of DNA synthesis as two replisomes converged within the *lacO* array. To minimize the loss of synchrony among replisomes after IPTG addition, we used a 365-bp array containing only 12 copies of *lacO*, which was sufficient to prevent dissolution at the 5 min time point (Extended Data Fig. 4c). We replicated p[$lacO_{12}$] in the presence of LacR, added IPTG after 5 min, and examined subsequent replication within the array by cutting the plasmid with AflIII and PvuII (Fig. 2a). The rate of DNA synthesis within the array was almost perfectly linear after IPTG addition (Fig. 2b, c) even as dissolution was underway. These data suggest that converging forks do not slow significantly before they meet. A similar conclusion was reached when radiolabelled nucleotides were added at the same time as IPTG and incorporation measured only during the final stage of replication on p[$lacO_{12}$] (Extended Data Fig. 5a–f) or p[$lacO_{16}$] (Extended Data Fig. 5g, h). Moreover, fork rates within the *lacO* array resembled those previously reported in the same egg extracts (Extended Data Fig. 5f). These results suggest that converging replisomes do not undergo prolonged stalling.

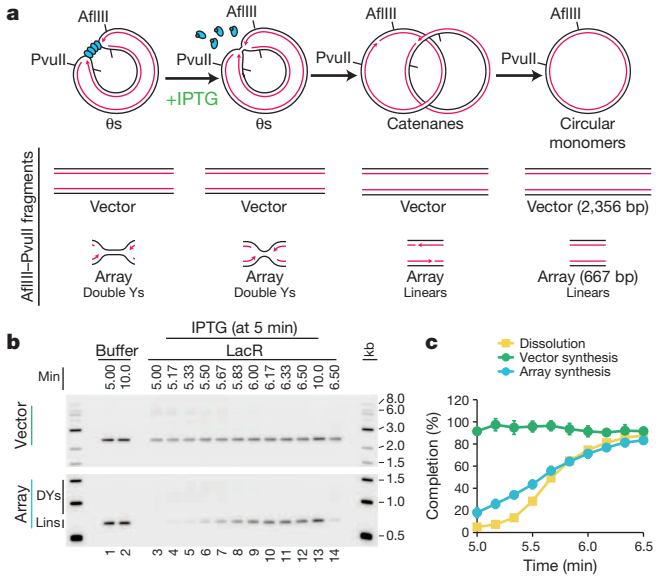


**Figure 2 | DNA synthesis does not stall during termination.** **a**, Cartoon depicting the assay for *lacO* array synthesis. **b**, LacR block-IPTG release was performed on p[$lacO_{12}$]. To measure synthesis within the array, termination intermediates were cut with AflIII and PvuII to liberate the array fragment from the vector. Cleaved products were separated by native gel electrophoresis. Different exposures of array and vector fragments are shown (see Methods). **c**, Array synthesis, vector synthesis and dissolution were quantified. Means ± s.d. are plotted ($n = 3$). kb, kilobase ladder, with the size of each band (in kilobases) labelled.

To evaluate further whether forks slow or stall upon encounter with a converging fork, we compared progression of leading strands into arrays containing 12 or 32 copies of *lacO* (Fig. 3a), in which the rightward fork should collide with a converging fork at the 6th or 16th *lacO* repeats, respectively (Fig. 3a). If converging forks interfere with each other, the rightward leading strand should pause or stall near the 6th repeat in p[$lacO_{12}$] but not in p[$lacO_{32}$]. As expected, dissolution (Fig. 1b) happened much earlier on p[$lacO_{12}$] than on p[$lacO_{32}$] (Extended Data Fig. 6a–d). To monitor leading-strand progression into the array with near-nucleotide resolution, DNA intermediates were purified, digested with the nicking enzyme Nt.BspQI, which released rightward leading strands (Fig. 3a), and separated on a denaturing polyacrylamide gel (Fig. 3b). Before IPTG addition, a discrete ladder of leading strands was seen (Fig. 3b, lanes 2, 14), in which the 3′ ends of leading strands stalled ~29–33 nt from each LacR molecule in the array. This ~30 nt gap probably corresponds to the footprint of the CMG complex[35,40]. As shown in Fig. 3b (red lines) and quantified in Extended Data Fig. 6e, 78% of leading strands were stalled at the first three *lacO* sites, indicating that most replisomes were blocked at the outer edges of the array.

Upon addition of IPTG, extension of leading strands resumed immediately (Fig. 3b, lanes 3–11 and 15–23). Notably, there was no enhanced pausing near the 6th *lacO* repeat of the $lacO_{12}$ array versus the $lacO_{32}$ array. By 5.67 min, most leading strands had extended beyond the 6th *lacO* repeat within both arrays (Fig. 3b, lanes 6 and 18, and Extended Data Fig. 2c). This was also true for the leftward leading strands (Extended Data Fig. 6f, g). Furthermore, leading strands were extended beyond the 6th *lacO* repeat in the $lacO_{12}$ and $lacO_{32}$ arrays with similar kinetics (Fig. 3c, d). When leading strands were analysed on alkaline denaturing gels, we observed that all rightward and leftward leading strands passed the mid-point of the array by 6.25 min (Extended Data Fig. 2d, e), indicating that the converging leading strands were readily extended past each other. In summary, we failed to observe detectable slowing or pausing of DNA synthesis during termination, and converging leading strands passed each other unhindered, implying that converging replisomes do not pause or stall significantly.

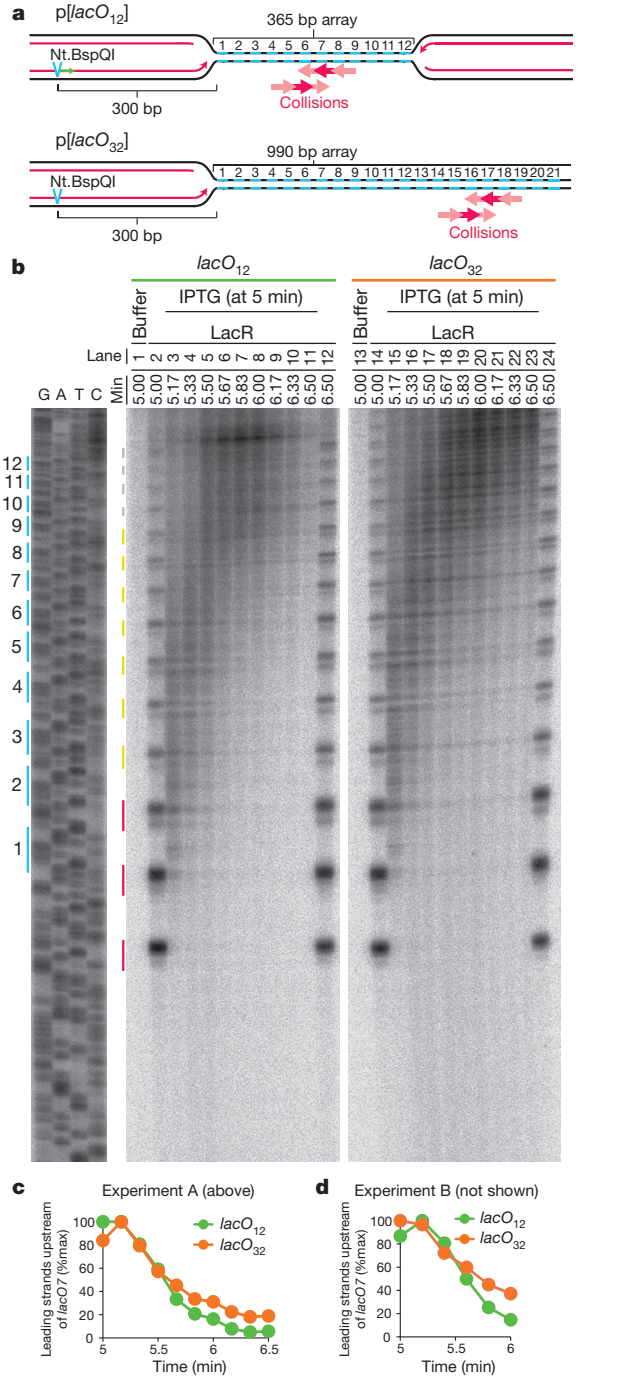


**Figure 3 | Leading strands pass each other unhindered during termination.** **a**, Schematic of rightward leading strands arrested at 12× and 32× *lacO* arrays ($lacO_{12}$ and $lacO_{32}$, respectively), and the predicted point of fork collision upon IPTG addition. **b**, LacR block-IPTG release was performed on p[$lacO_{12}$] and p[$lacO_{32}$]. Termination intermediates were digested with Nt.BspQI. Nascent strands were separated alongside a sequencing ladder (generated by primer JDO107, green arrow in **a**) on a denaturing polyacrylamide gel and visualized by autoradiography. The *lacO* sites of p[$lacO_{12}$] are indicated in blue. Red, yellow and grey lines indicate stall products that were quantified (Extended Data Fig. 6e). **c**, Leading strands whose 3′ ends were located before *lacO7* were quantified (see Methods) along with dissolution (Extended Data Fig. 6a–d). **d**, Experimental repeat of **c**.

## Lagging strand gaps are rapidly filled in

During SV40 replication termination, gaps of ~60 nt persist after dissolution[11]. To determine whether the appearance of such gaps precedes the ligation step in our system, we mapped the 3′ ends of

the leftward leading strands and the 5′ ends of the rightward lagging strands during termination within $lacO_{12}$ (Fig. 4a). To this end, we digested DNA intermediates with Nb.BbvCI or Nb.BtsI to release leading or lagging strands, respectively (Fig. 4a), and separated them on denaturing polyacrylamide gels. After IPTG addition, we detected a prominent leading-strand product beyond the 12th *lacO* repeat (species 274 in Fig. 4b; the 3′ and 5′ termini of all leading and lagging strand products, respectively, are mapped relative to the Nb.BtsI site) as seen also in Fig. 3b. The 3′ end of this species was located ~3 nt from the 5′ end of the most abundant lagging strand product of the converging fork (271, Fig. 4c). We observed many other, less prominent, leading-strand products (181–420, Fig. 4b), most of which mapped close to corresponding lagging strand products (176–417, Fig. 4c). The results show that leading strands are generally extended to within ~3 nt of the lagging strands (Fig. 4d). It is likely that leading strands immediately abut lagging strands and that the ~3 nt gap reflects imprecise mapping of lagging strands (see Methods). In conclusion, we observed no evidence of persistent gaps between leading and lagging strands during replication termination.

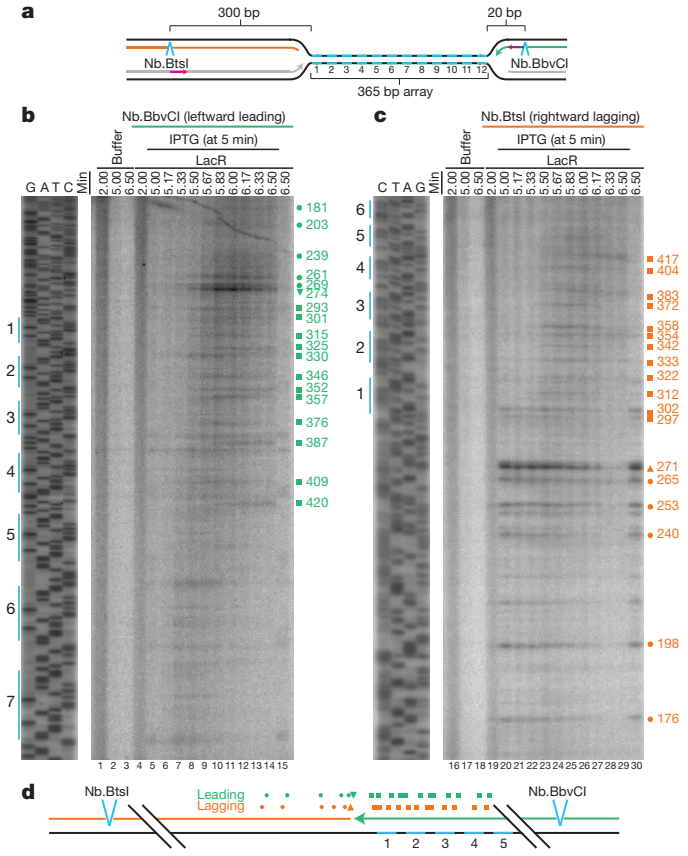


**Figure 4 | Leading strands abut lagging strands of the opposing replisome during termination.** **a**, Cartoon illustrating the leading and lagging strands released by Nb.BtsI and Nb.BbvCI nicking enzymes. Primers JDO111 (purple arrow) and JDO110 (pink arrow) generated the sequencing ladders in **b** and **c**, respectively. **b**, LacR block-IPTG release was performed on p[$lacO_{12}$]. Termination intermediates were digested with Nb.BbvCI to liberate leftward leading strands, which were separated alongside a sequencing ladder on a denaturing polyacrylamide gel and visualized by autoradiography. Prominent leading strand products are highlighted (green symbols), and their sizes, in nucleotides, measured relative to the Nb.BtsI site, are indicated. **c**, Same samples as in **b** were digested with Nb.BtsI to liberate rightward lagging strands. The size of prominent lagging strand products (orange symbols), measured relative to the Nb.BtsI site, are indicated. **d**, Schematic of the mapped leading (**b**) and lagging (**c**) strands.

## CMGs dissociate late during termination

To determine when replisome components dissociate during termination, we monitored MCM7, CDC45, Polε and RPA binding to a site flanking the *lacO* array using chromatin immunoprecipitation (ChIP) (*FLK2* locus, Extended Data Fig. 7a). In parallel, we monitored dissolution, ligation and decatenation. Before IPTG addition, MCM7, CDC45, Polε and RPA were 4–8-fold enriched at the array in the presence of LacR compared to buffer (Extended Data Fig. 7b–e, 5 min time point), demonstrating that the ChIP signal reflects replisome stalling at the array. When IPTG was added at 5 min, MCM7, CDC45, RPA and Polε largely dissociated by 9 min, whereas in the absence of IPTG, they dissociated much more slowly (Extended Data Fig. 7b–e). RPA dissociation correlated well with ligation, as expected, since ligation marks the disappearance of any single-stranded (ss)DNA in the termination zone (Fig. 5a, compare red squares and blue circles). Notably, CDC45, MCM7 and Polε dissociated ~1.5 min after dissolution and ~0.5 min after RPA dissociation and ligation (Fig. 5a). A time course of ChIP at sequences adjacent to and within the array (Extended Data Fig. 7f–i) was consistent with MCM7, CDC45 and DNA Polε moving into the array and then back out after dissolution (Extended Data Fig. 7j). MCM7 and CDC45 also dissociated after dissolution during replication of plasmid DNA that lacked a *lacO* array (p[empty], Extended Data Fig. 8a, b). Although the delay between ligation and unloading of MCM7 and CDC45 was not readily detectable on this template (Extended Data Fig. 8b), this was not surprising, given the asynchrony of termination in this setting. Together, the data support a model in which CDC45 and MCM7 dissociate late in termination, long after forks meet (dissolution) and shortly after ligation.

If our model is correct, inhibiting CMG unloading should not affect dissolution or ligation. To test this, we inhibited ubiquitin signalling, which is required for chromatin dissociation of CMG[24,25,41]. p[empty] was replicated in extracts that were incubated with vehicle or the deubiquitylating enzyme inhibitor ubiquitin-vinyl-sulfone (Ub-VS), which leads to the depletion of free ubiquitin[35,41], and we performed MCM7 and CDC45 ChIP. As shown in Fig. 5b, c, Ub-VS substantially delayed MCM7 and CDC45 dissociation, and this effect was partially reversed by co-addition of free ubiquitin (Fig. 5b, c). The same inhibitory effect of Ub-VS on CMG unloading was observed when plasmids were recovered from egg extract and blotted for MCM7 and CDC45 (Extended Data Fig. 8c). This analysis also confirmed previous reports[24,25] of MCM7 ubiquitylation during replication (Extended Data Fig. 8c). Importantly, dissolution, ligation and decatenation were not affected by Ub-VS (Fig. 5d, e and Extended Data Fig. 8f–i). We conclude that defective CMG unloading does not affect dissolution, ligation, or decatenation, strongly supporting our model that CMG unloading is a late event in replication termination.

## Discussion

We present a novel approach to induce synchronous and site-specific replication termination. Using this system, we observe no slowing or pausing of DNA synthesis as forks converge (Fig. 5f, panels i, ii). Leading strands pass each other unhindered and immediately abut downstream lagging strands before undergoing ligation (Fig. 5f, panels iii–v). CMG remains associated with DNA after dissolution, and it is unloaded only after the leading strand of one fork is ligated to the lagging strand of the opposing fork (Fig. 5f, panel vii). Catenane removal is initiated at the same time as ligation (Fig. 5f, panels v, vi). In contrast to models of termination in which replication forks stall[1,3,4], our data imply that topological stress between replisomes is handled efficiently and that converging replisomes do not clash or that if they do, any remaining template DNA is immediately reeled into the stalled replisome for duplication (not shown). We previously showed that CMGs encircle the leading strand template at the replication fork[42]. Therefore, converging CMGs approach each other on opposite strands[42,43], which helps explain how they could pass each other. If a

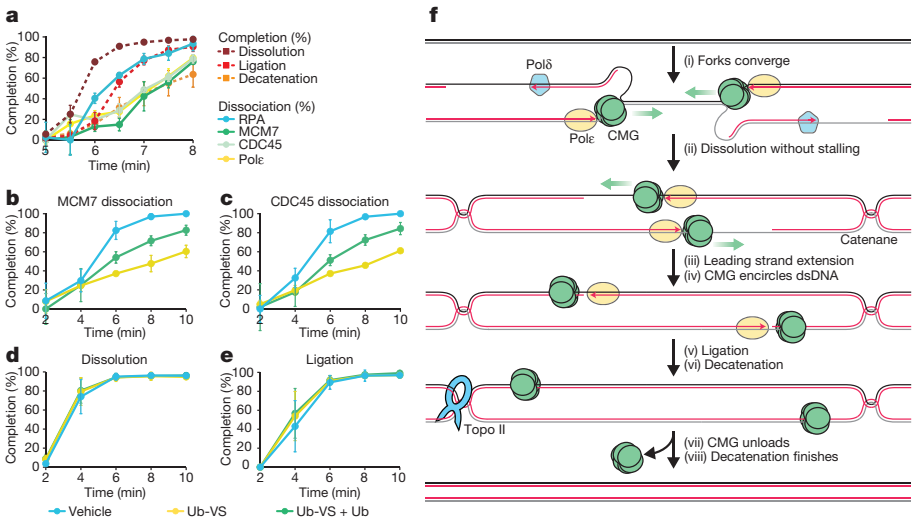


**Figure 5 | CMGs dissociate after dissolution and ligation.** **a**, LacR block-IPTG release was followed by MCM7, CDC45, RPA and Polε ChIP at the indicated times after IPTG addition. Dissolution, ligation and decatenation were measured in parallel. Means ± s.d. are plotted ($n = 3$). **b**, p[empty] was replicated in extracts treated with vehicle, ubiquitin-vinyl sulfone (Ub-VS), or Ub-VS and free ubiquitin (Ub-VS + Ub). Dissociation of MCM7 was measured by ChIP (see Methods). Mean ± s.d. is plotted ($n = 3$). **c**, Same as **b** but CDC45 dissociation was measured. **d**, **e**, In parallel to MCM7 and CDC45 dissociation (**b**, **c**), dissolution (**d**) and ligation (**e**) were measured. Mean ± s.d. is plotted ($n = 3$). See Extended Data Fig. 8f–i for decatenation measurements and representative gels. **f**, New model of vertebrate replication termination.

fork stalls (for example, at the ribosomal DNA locus[13,14]), the same termination mechanism could still operate provided that the stalled fork remains stable until a converging fork arrives. We expect this to be the case, given our recent observation that a single fork stalled at a DNA interstrand cross-link does not collapse or lose its CMG complex[34]. We speculate that at telomeres the replisome simply runs off the chromosome end.

Our observations that CMG dissociates after the ligation step (Fig. 5a), and that ligation is not affected when CMG unloading is impaired (Fig. 5b, c, e), strongly imply that CMG is unloaded from dsDNA. We propose that when CMG reaches the 5′ end of the opposing fork's lagging strand, it passes over the ssDNA–dsDNA junction and keeps moving along dsDNA (Fig. 5f), as previously observed for purified MCM2–7 and CMG *in vitro* (see refs 23, 44 but see also ref. 22). This scenario is appealing, as it would prevent CMG from interfering with ligation of the nascent strands. We propose that CMG ubiquitylation and its removal by p97 (refs 24, 25) is triggered once CMG encircles dsDNA. Such a mechanism would help to avoid inappropriate CMG unloading from active replication forks, where CMG encircles ssDNA. Our results disagree with a recent report, which concluded that inhibition of CMG unloading prevents completion of DNA synthesis[25]. In contrast, another report that defective CMG unloading does not prevent cell cycle progression[24] is consistent with our model. We recently reported that CMG can be unloaded from ssDNA when two replisomes collide with a DNA interstrand cross-link[41]. However, this process involves a unique, BRCA1-dependent pathway that is not employed during termination[41]. In conclusion, the termination mechanism described here allows rapid completion of DNA synthesis while minimizing the possibility of premature replisome disassembly.

**Online Content** Methods, along with any additional Extended Data display items and Source Data, are available in the online version of the paper; references unique to these sections appear only in the online paper.

**Received 27 September 2014; accepted 1 July 2015.**
**Published online 31 August 2015.**

1. Levene, A. J., Kang, H. S. & Billheimer, F. E. DNA replication in SV40 infected cells. I. Analysis of replicating SV40 DNA. *J. Mol. Biol.* **50,** 549–568 (1970).
2. Fanning, E. & Zhao, K. SV40 DNA replication: from the A gene to a nanomachine. *Virology* **384,** 352–359 (2009).
3. Tapper, D. P. & DePamphilis, M. L. Discontinuous DNA replication: Accumulation of simian virus 40 DNA at specific stages in its replication. *J. Mol. Biol.* **120,** 401–422 (1978).
4. Seidman, M. M. & Salzman, N. P. Late replicative intermediates are accumulated during simian virus 40 DNA replication *in vivo* and *in vitro*. *J. Virol.* **30,** 600–609 (1979).
5. Sundin, O. & Varshavsky, A. Terminal stages of SV40 DNA replication proceed via multiply intertwined catenated dimers. *Cell* **21,** 103–114 (1980).
6. Ishimi, Y., Sugasawa, K., Hanaoka, F., Eki, T. & Hurwitz, J. Topoisomerase II plays an essential role as a swivelase in the late stage of SV40 chromosome replication *in vitro*. *J. Biol. Chem.* **267,** 462–466 (1992).
7. Hiasa, H. & Marians, K. J. Two distinct modes of strand unlinking during theta-type DNA replication. *J. Biol. Chem.* **271,** 21529–21535 (1996).
8. Espeli, O., Levine, C., Hassing, H. & Marians, K. J. Temporal regulation of topoisomerase IV activity in *E. coli*. *Mol. Cell* **11,** 189–201 (2003).
9. Segawa, M., Sugano, S. & Yamaguchi, N. Association of simian virus 40 T antigen with replicating nucleoprotein complexes of simian virus 40. *J. Virol.* **35,** 320–330 (1980).
10. Tack, L. C. & DePamphilis, M. L. Analysis of simian virus 40 chromosome-T-antigen complexes: T-antigen is preferentially associated with early replicating DNA intermediates. *J. Virol.* **48,** 281–295 (1983).
11. Chen, M. C., Birkenmeier, E. & Salzman, N. P. Simian virus 40 DNA replication: characterization of gaps in the termination region. *J. Virol.* **17,** 614–621 (1976).
12. Sundin, O. & Varshavsky, A. Arrest of segregation leads to accumulation of highly intertwined catenated dimers: dissection of the final stages of SV40 DNA replication. *Cell* **25,** 659–669 (1981).
13. Ivessa, A. S., Zhou, J. Q. & Zakian, V. A. The *Saccharomyces* Pif1p DNA helicase and the highly related Rrm3p have opposite effects on replication fork progression in ribosomal DNA. *Cell* **100,** 479–489 (2000).
14. Steinacher, R., Osman, F., Dalgaard, J. Z., Lorenz, A. & Whitby, M. C. The DNA helicase Pfh1 promotes fork merging at replication termination sites to ensure genome stability. *Genes Dev.* **26,** 594–602 (2012).
15. Fachinetti, D. *et al.* Replication termination at eukaryotic chromosomes is mediated by Top2 and occurs at genomic loci containing pausing elements. *Mol. Cell* **39,** 595–605 (2010).
16. DiNardo, S., Voelkel, K. & Sternglanz, R. DNA topoisomerase II mutant of *Saccharomyces cerevisiae*: topoisomerase II is required for segregation of daughter molecules at the termination of DNA replication. *Proc. Natl Acad. Sci. USA* **81,** 2616–2620 (1984).
17. Baxter, J. & Diffley, J. F. Topoisomerase II inactivation prevents the completion of DNA replication in budding yeast. *Mol. Cell* **30,** 790–802 (2008).
18. Lucas, I., Germe, T., Chevrier-Miller, M. & Hyrien, O. Topoisomerase II can unlink replicating DNA by precatenane removal. *EMBO J.* **20,** 6509–6519 (2001).
19. Gaggioli, V., Le Viet, B., Germe, T. & Hyrien, O. DNA topoisomerase II controls replication origin cluster licensing and firing time in *Xenopus* egg extracts. *Nucleic Acids Res.* **41,** 7313–7331 (2013).
20. Ilves, I., Petojevic, T., Pesavento, J. J. & Botchan, M. R. Activation of the MCM2–7 helicase by association with Cdc45 and GINS proteins. *Mol. Cell* **37,** 247–258 (2010).
21. Pacek, M., Tutter, A. V., Kubota, Y., Takisawa, H. & Walter, J. C. Localization of MCM2–7, Cdc45, and GINS to the site of DNA unwinding during eukaryotic DNA replication. *Mol. Cell* **21,** 581–587 (2006).
22. Moyer, S. E., Lewis, P. W. & Botchan, M. R. Isolation of the Cdc45/Mcm2–7/GINS (CMG) complex, a candidate for the eukaryotic DNA replication fork helicase. *Proc. Natl Acad. Sci. USA* **103,** 10236–10241 (2006).
23. Kang, Y. H., Galal, W. C., Farina, A., Tappin, I. & Hurwitz, J. Properties of the human Cdc45/Mcm2–7/GINS helicase complex and its action with DNA polymerase ε in rolling circle DNA synthesis. *Proc. Natl. Acad. Sci. USA* **109,** 6042–6047 (2012).
24. Maric, M., Maculins, T., De Piccoli, G. & Labib, K. Cdc48 and a ubiquitin ligase drive disassembly of the CMG helicase at the end of DNA replication. *Science* **346,** 1253596–1253596 (2014).
25. Priego Moreno, S., Bailey, R., Campion, N., Herron, S. & Gambus, A. Polyubiquitylation drives replisome disassembly at the termination of DNA replication. *Science* **346,** 477–481 (2014).
26. Hiasa, H. & Marians, K. J. Tus prevents overreplication of oriC plasmid DNA. *J. Biol. Chem.* **269,** 26959–26968 (1994).

27. Rudolph, C. J., Upton, A. L., Stockum, A., Nieduszynski, C. A. & Lloyd, R. G. Avoiding chromosome pathology when replication forks collide. *Nature* **500,** 608–611 (2013).
28. Hook, S. S., Lin, J. J. & Dutta, A. Mechanisms to control rereplication and implications for cancer. *Curr. Opin. Cell Biol.* **19,** 663–671 (2007).
29. Czajkowsky, D. M., Liu, J., Hamlin, J. L. & Shao, Z. DNA combing reveals intrinsic temporal disorder in the replication of yeast chromosome VI. *J. Mol. Biol.* **375,** 12–19 (2008).
30. McGuffee, S. R., Smith, D. J. & Whitehouse, I. Quantitative, genome-wide analysis of eukaryotic replication initiation and termination. *Mol. Cell* **50,** 123–135 (2013).
31. Yardimci, H., Loveland, A. B., Habuchi, S., van Oijen, A. M. & Walter, J. C. Uncoupling of sister replisomes during eukaryotic DNA replication. *Mol. Cell* **40,** 834–840 (2010).
32. Loveland, A. B., Habuchi, S., Walter, J. C. & van Oijen, A. M. A general approach to break the concentration barrier in single-molecule imaging. *Nature Methods* **9,** 987–992 (2012).
33. Santamaría, D. *et al.* Bi-directional replication and random termination. *Nucleic Acids Res.* **28,** 2099–2107 (2000).
34. Zhang, J. *et al.* DNA interstrand cross-link repair requires replication fork convergence. *Nature Struct. Mol. Biol.* **22,** 242–247 (2015).
35. Duxin, J. P. P., Dewar, J. M. M., Yardimci, H. & Walter, J. C. C. Replication-coupled repair of a DNA-protein crosslink. *Cell* **159,** 346–357 (2014).
36. Walter, J., Sun, L. & Newport, J. Regulated chromosomal DNA replication in the absence of a nucleus. *Mol. Cell* **1,** 519–529 (1998).
37. Sofueva, S. *et al.* Ultrafine anaphase bridges, broken DNA and illegitimate recombination induced by a replication fork barrier. *Nucleic Acids Res.* **39,** 6568–6584 (2011).
38. Charbin, A., Bouchoux, C. & Uhlmann, F. Condensin aids sister chromatid decatenation by topoisomerase II. *Nucleic Acids Res.* **42,** 340–348 (2014).
39. Laskey, R. A., Mills, A. D. & Morris, N. R. Assembly of SV40 chromatin in a cell-free system from *Xenopus* eggs. *Cell* **10,** 237–243 (1977).
40. Räschle, M. *et al.* Mechanism of replication-coupled DNA interstrand crosslink repair. *Cell* **134,** 969–980 (2008).
41. Long, D. T. T., Joukov, V., Budzowska, M. & Walter, J. C. C. BRCA1 promotes unloading of the CMG helicase from a stalled DNA replication fork. *Mol. Cell* **56,** 174–185 (2014).
42. Fu, Y. V. *et al.* Selective bypass of a lagging strand roadblock by the eukaryotic replicative DNA helicase. *Cell* **146,** 931–941 (2011).
43. Costa, A. *et al.* The structural basis for MCM2–7 helicase activation by GINS and Cdc45. *Nature Struct. Mol. Biol.* **18,** 471–477 (2011).
44. Kaplan, D. L., Davey, M. J. & O'Donnell, M. Mcm4,6,7 uses a 'pump in ring' mechanism to unwind DNA by steric exclusion and actively translocate along a duplex. *J. Biol. Chem.* **278,** 49171–49182 (2003).

**Acknowledgements** We thank C. Richardson and members of the Walter laboratory for feedback on the manuscript. We thank K. J. Marians and J. T. Yeeles for plasmids and the LacI purification protocol. J.C.W. was supported by NIH grants GM62267 and GM80676. J.C.W. is an investigator of the Howard Hughes Medical Institute.

**Author Contributions** J.M.D. and J.C.W. designed the experiments. J.M.D. performed the experiments. M.B. developed methodologies for plasmid pull downs and $HIS_6$-Ub immunoprecipitations. J.M.D. and J.C.W. interpreted the data and wrote the paper.

**Author Information** Reprints and permissions information is available at www.nature.com/reprints. The authors declare no competing financial interests. Readers are welcome to comment on the online version of the paper. Correspondence and requests for materials should be addressed to J.C.W. (johannes_walter@hms.harvard.edu).

## METHODS

No statistical methods were used to predetermine sample size.

**Protein purification.** Biotinylated LacR was purified using a protocol adapted from Kenneth Marian's laboratory (personal communication). The LacR open reading frame was fused to a C-terminal AviTag (Avidity, Denver, CO) and expressed from pET11a (pET11a[LacR-Avi]). To biotinylate the AviTag on LacR-Avi, biotin ligase was co-expressed from pBirAcm (Avidity, Denver, CO). To this end, pET11a[LacR-Avi] and pBirAcm were co-transformed into T7 Express cells (New England Biolabs) and grown in the presence of ampicillin (100 μg ml$^{-1}$) and chloramphenicol (17 μg ml$^{-1}$). Expression of LacR-Avi and the biotin ligase was induced by addition of IPTG to a final concentration of 1 mM. Cultures were supplemented with 50 μM biotin (Research Organics, Cleveland, OH) to ensure efficient biotinylation of LacR-Avi.

Cell pellets were resuspended in lysis buffer (50 mM Tris-HCl, pH 7.5, 5 mM EDTA, 100 mM NaCl, 1 mM DTT, 10% sucrose (w/v), Complete protease inhibitor (Roche, Nutley, NJ)). The cells were lysed at room temperature in the presence of 0.2 mg ml$^{-1}$ lysozyme and 0.1% Brij 58. The insoluble, chromatin-containing fraction was isolated by centrifugation at 4 °C. Chromatin-bound LacR was then released by sonication (in 50 mM Tris-HCl, pH 7.5, 5 mM EDTA, 1 M NaCl, 1 mM DTT, Complete protease inhibitor, 30 mM IPTG). DNA was removed from the soluble fraction by addition of polymin P (final concentration 1%), LacR was precipitated by addition of ammonium sulfate (final concentration 37%). The precipitate was dissolved in wash buffer (50 mM Tris-HCl, pH 7.5, 1 mM EDTA, 2.5 M NaCl, 1 mM DTT, Complete protease inhibitor) and then applied to a column of SoftLink avidin resin (Promega, Madison, WI). LacR was eluted (in 50 mM Tris-HCl, pH 7.5, 1 mM EDTA, 100 mM NaCl, 1 mM DTT, 5 mM biotin) and dialysed overnight (against 50 mM Tris-HCl, pH 7.5, 1 mM EDTA, 150 mM NaCl, 1 mM DTT, 38% glycerol (v/v)). Purified LacR was frozen in liquid nitrogen and stored at −80 °C. A more detailed purification protocol is available on request.

Cyclin A was purified as described previously[45].

**Plasmid construction and preparation.** pJD82 (Extended Data Table 1) was created by replacing the SacI-KpnI fragment of pBlueScript II KS- with the sequence: GAGCTCTCACACCTACAAGGGATGTACATCAATTGTGAGCG GATAACAATTGTTAGGGAGGAATTGTGAGCGGATAACAATTTGGAGT TGATAATTGTGAGCGGATAACAATTGGCTTCAACGTAATTGTGAGCGG ATAACAATTTCCGTACGAATGTGCCGAACTTATGGTACC. This contains four tandem repeats of the *lac* operator sequence (AATTGTGAGCGGATAA CAATT) interspersed by an average of 10–11 bp of random sequence (average 10.33 bp). Additional tandem repeats of the BsiWI-BsrGI fragment were then cloned into pJD82, and subsequently derived vectors, to generate arrays of 8, 12, 16, 32 and 48 *lacO* repeats (Extended Data Table 1). Recognition sites for nicking enzymes were introduced by QuickChange mutagenesis (Agilent Technologies, Santa Clara, CA) according to the manufacturer's guidelines.

To propagate *lacO* plasmid DNA, plasmids were transformed into DH5α cells and grown for a minimal number of passages in the presence of 2 mM IPTG. DNA was prepared using the QIAprep spin kit (Qiagen, Valencia, CA). To eliminate preparations containing genetic rearrangements (typically ~25%), each preparation was separated by electrophoresis on a 0.8% agarose gel and visualized by ethidium bromide staining. Preparations that were free of rearranged plasmids were then verified by sequencing (Genewiz, Cambridge, MA).

***Xenopus* egg extracts and DNA replication.** *Xenopus* egg extracts were prepared from *Xenopus laevis* wild-type males and females 2–5 years of age, as approved by the Harvard Medical School Institutional Animal Care and use Committee (IACUC) and as described previously[46]. For DNA replication, 1 volume of 'licensing mix' was prepared by adding plasmid DNA to High Speed Supernatant (HSS) of egg cytoplasm to a final concentration of 7.5–15 ng μl$^{-1}$. Licensing mix was incubated for 30 min at room temperature, leading to the formation of pre-replication complexes (pre-RCs). Next, licensing mix was supplemented with 0.1 volumes of cyclin A to a final volume of 576 nM and incubated a further 10 min at room temperature, as previously described[45]. Cyclin A treatment was performed to achieve highly synchronous DNA replication (Extended Data Fig. 9). Finally, 1.9 volumes of nucleoplasmic extract (NPE) was added to initiate Cdk2-dependent replication at pre-RCs. In all figures, '0 minutes' represents the time 30 s after NPE addition. To radiolabel DNA, NPE was supplemented with [α-$^{32}$P]dATP. Reactions were stopped with 10 volumes Stop Solution (0.5% SDS, 25 mM EDTA, 50 mM Tris-HCl pH 7.5). DNA in Stop Solution was treated with RNase A (190 ng μl$^{-1}$ final concentration) then Proteinase K (909 ng μl$^{-1}$ final concentration) before either direct analysis by gel electrophoresis or purification of DNA as described previously[40]. For Ub-VS experiments, Ub-VS (Boston Biochem) was added to final concentration of 20 μM, to HSS 5 min before addition of plasmid DNA (HSS) and to NPE 5 min before addition of HSS, with or without 120 μM ubiquitin (Boston Biochem). Unless otherwise stated in the figure legend, all experiments were performed at least twice and a representative result is shown. Replicate samples were collected from independently assembled replication reactions, and therefore represent biological replicates.

**Immunodepletions.** To deplete Topo II-α from *Xenopus* egg extracts one volume of Protein A Sepharose Fast Flow (PAS) (GE Healthcare) was incubated with 4.5 volumes of affinity purified, anti-Topo II-α antibody raised against the C-terminal 20 residues (1 mg ml$^{-1}$). For mock depletion, an equivalent quantity of nonspecific IgGs was used. Five volumes of pre-cleared HSS or NPE was then mixed with one volume of the antibody-bound sepharose and incubated for 45 min at 4 °C, and for the NPE this was repeated once. Depleted extracts were collected and used immediately for DNA replication.

**Induction of termination.** To monitor termination, 0.05 volumes of plasmid DNA (150–300 ng μl$^{-1}$) was incubated with 0.1 volumes LacR (54 μM) or dialysis buffer for at least 90 min at room temperature to allow formation of LacR arrays on the DNA. Licensing mix was prepared by adding 0.85 volumes of HSS, and DNA was replicated as described above. To induce termination, 0.06 volumes of IPTG was added (to a final concentration of 10 mM) at the time indicated (typically 5 min), which triggered dissociation of *lacO*-bound LacR. To accurately withdraw samples at the times indicated, reactions composed of the same Licensing Mix and NPE were staggered, where necessary.

**2D gel electrophoresis.** 2D gels were performed as described[41]. Briefly, purified DNA was digested with XmnI (New England BioLabs) and then separated by native–native 2D gel electrophoresis. Samples were separated in the first dimension on a 0.4% agarose gel at 0.75 volts (V) cm$^{-1}$ for approximately 40 h at room temperature. The gel was stained with 0.3 μg ml$^{-1}$ ethidium bromide, allowing the 2–8 kb size range to be excised. A second dimension gel containing 1% agarose and 0.3 μg ml$^{-1}$ ethidium bromide was cast over the gel slice from the first dimension. DNA was separated on the second dimension at 4.5 V cm$^{-1}$ for 12 h at 4 °C.

**Termination assays.** To monitor dissolution, 0.25–1.0 ng μl$^{-1}$ of purified DNA was incubated in CutSmart Buffer with 0.4 units μl$^{-1}$ of XmnI (New England BioLabs) at 37 °C for 1 h. Digested products were separated on a 1.2% agarose gel at 4 V cm$^{-1}$ and detected by autoradiography. Dissolution (%) was calculated as the percentage of total signal in each lane present in the linear products of digestion (Lins, Fig. 1c).

To monitor ligation, 0.25–1.0 ng μl$^{-1}$ of purified DNA was incubated in CutSmart buffer with 0.2 units μl$^{-1}$ of AlwNI (New England BioLabs) at 37 °C for 1 h. Digests were terminated by addition of EDTA to 30 mM, then products were separated on a 1.5% denaturing alkaline agarose gel at 1.5 V cm$^{-1}$ and detected by autoradiography. The percentage of total signal in each lane present in the full-length strands was measured (FLS, Fig. 1e). During electrophoresis, partial hydrolysis caused signal from the FLS to smear down. To correct for this, a fully ligated plasmid was cleaved and analysed on the same gel. The percentage of signal in FLS band of the fully ligated plasmid was measured (FLS$^{FL}$) and used to correct signal in the other lanes to yield an accurate measure of ligation. Ligation (%) was calculated as FLS/FLS$^{FL}$ × 100,

To monitor decatenation, 0.25–1.0 ng μl$^{-1}$ of purified DNA was separated on a 0.8% agarose gel at 4 V cm$^{-1}$ and detected by autoradiography. Decatenation (%) was measured as the percentage of total signal in each lane present in circular monomers (CMs, Fig. 1g).

To monitor DNA synthesis within a *lacO* array (Fig. 2), 0.25–1.0 ng μl$^{-1}$ of purified DNA was incubated in buffer 3.1 with 0.2 units μl$^{-1}$ PvuII and 0.2 units μl$^{-1}$ AflIII (New England BioLabs) at 37 °C for 1 h. Digested products were separated on a 1.2% agarose gel at 4 V cm$^{-1}$ and detected by autoradiography. To measure array synthesis (SYN$^{ARY}$), the 0.5–1.5-kb region of each lane was quantified (lins and DYs, Fig. 2b). To measure vector synthesis (SYN$^{VEC}$), the 2–6 kb region of each lane was quantified, which included the ~3.0 and ~6.0 bands that arose when one, or both, lagging strands did not cut, respectively. Total signal in each lane (SYN$^{TOT}$) was also measured. To correct for differences in efficiency of DNA extraction, total lane signal was also measured in a set of unprocessed samples (SYN$^{UN}$), which were separated and detected in parallel. Array synthesis (%) was calculated as SYN$^{UN}$/SYN$^{TOT}$ × SYN$^{ARY}$, vector synthesis was calculated as SYN$^{UN}$/SYN$^{TOT}$ × SYN$^{VEC}$ and in both cases the 10 min time point was assigned a value of 100%. The same approach was also used to quantify synthesis of the 294/794 bp fragments (quantified in the same manner as the array) and the 2,354 bp fragments (quantified in the same manner as the vector fragments) in Extended Data Fig. 1. In Fig. 2 and Extended Data Fig. 1, a longer exposure of the array fragment is shown because it is less intense than the vector fragment.

To analyse topoisomers (Extended Data Fig. 3d), 0.25 ng μl$^{-1}$ of radiolabelled DNA was incubated in 1× buffer A and 1× buffer B (Topogen) with 0.2 U μl$^{-1}$

Human Topo II-α (Topogen) at 37 °C for 15 min, or in CutSmart buffer with 0.4 U $\mu l^{-1}$ XmnI or 0.04 U $\mu l^{-1}$ Nt.BspQI (New England Biolabs) for 1 h.

**Nascent strand analysis.** To nick rightward leading strands, 1–2 ng $\mu l^{-1}$ of purified DNA was incubated in buffer 3.1 with 0.4 units $\mu l^{-1}$ Nt.BspQI (New England BioLabs) at 37 °C for 1 h. To nick leftward leading strands, 1–2 ng μl of purified DNA was incubated in CutSmart buffer with 0.04 units $\mu l^{-1}$ Nb.BsrDI (New England BioLabs) at 65 °C for 1 h. To nick rightward leading strands closer to the *lacO* array, 1–2 ng $\mu l^{-1}$ of purified DNA was incubated in CutSmart buffer with 0.04 units $\mu l^{-1}$ Nb.BbvCI (New England BioLabs) at 37 °C for 1 h. To nick leftward lagging strands, 1–2 ng $\mu l^{-1}$ of purified DNA was incubated in buffer 3.1 with 0.04 units $\mu l^{-1}$ Nb.BtsI (New England BioLabs) at 37 °C for 1 h. In all cases, nicking reactions were stopped by the addition of 0.5 volumes of Stop solution B (95% formamide, 20 mM EDTA, 0.05% bromophenol blue, 0.05% xylene cyanol FF).

Nicked DNA (1.5–2 μl sample) was separated on a 42-cm-long 4% or 5% polyacrylamide sequencing gel using Model S2 sequencing gel apparatus (Apogee Electrophoresis, Baltimore, MD) according to the manufacturer's guidelines. To maximize the range of nascent products that could be resolved, gels were cast with a thickness gradient of 0.4 to 1.2 mm, beginning to end, to establish an electrical field gradient during electrophoresis. Sequencing gels were prepared with Rapidgel-XL in 0.8× GTG buffer (USB Corporation, Cleveland). Sequencing ladders were generated using the Cycle Sequencing Kit (USB Corporation, Cleveland) with primers JDO107, JDO109, JDO110, JDO111 (Extended Data Table 1) and pJD150 (Extended Data Table 1) as template DNA.

Mapping and quantification of the nascent strands in Figs 3 and 4 was performed as follows. Nascent leading and lagging strands were mapped using the sequencing ladders generated by the primers indicated in Fig. 3a and Fig. 4a (see Extended Data Table 1 for sequences). Slight discrepancies may exist between mapped and actual lagging strand product sizes (Fig. 4c) since the sequencing ladder (generated by JDO110 Fig. 4a) is complementary to the lagging strands. A fraction of lagging strand products 176–302 were not extended upon IPTG addition, probably because they were reached by the rightward leading strand first. Lagging strand products 312–417 appeared *de novo* after IPTG addition, and therefore represent growing lagging strands of the leftward fork. To quantify leading strand progression (Fig. 3c, d), leading strands whose 3′ ends were located before *lacO7* (in Fig. 3b and data not shown) were quantified, and peak signal was assigned a value of 100 (%Max).

**ChIP and quantitative PCR.** ChIP and quantitative PCR (qPCR) were performed essentially as described[41]. Chromatin was withdrawn and crosslinked in the presence of 1% formaldehyde for 10 min at room temperature. Crosslinking was then quenched by the addition of 0.1 volumes glycine (1.25 M) for 10 min. Samples were then spun through Bio-Spin P-6 Gel (containing Tris Buffer, Bio-Rad) to remove salts and small molecules, before being stored in 10 volumes of sonication buffer (20 mM Tris pH 7.5, 150 mM NaCl, 2 mM EDTA, 1% IGEPAL CA-630 (v/v), 2 mM PMSF, 5 μg $\mu l^{-1}$ aprotinin, 5 μg $\mu l^{-1}$ leupeptin). Samples were then sonicated to shear chromatin into approximately 250 bp fragments.

The antibodies used were described previously[21,41]. Antibodies were incubated with chromatin overnight at 4 °C, then immunoprecipitated by addition of Protein A-Sepharose Fast Flow beads (GE Healthcare) for 2 h at room temperature. Beads were washed sequentially with sonication buffer, high salt buffer (sonication buffer supplemented with 500 mM NaCl and 100 mM KCl), wash buffer (10 mM Tris pH 7.5, 0.25 M LiCl, 1 mM EDTA, 0.5% NP-40 (v/v), 0.5% SDS (w/v)) and TE (10 mM Tris pH 7.5, 1 mM EDTA), before being eluted into elution buffer (50 mM Tris pH 7.5, 10 mM EDTA, 1% SDS) at 65 °C for 20 min. Eluted chromatin, and input samples, were treated with RNase for 30 min at 37 °C. Finally, proteins were degraded by addition of NaCl (250 mM final) and treatment with Pronase (2 μg $\mu l^{-1}$ final) at 42 °C for 6 h. DNA-peptide crosslinks were reversed by treatment at 70 °C for a further 9 h. DNA was subsequently phenol:chloroform extracted and ethanol precipitated. The absolute amount of DNA recovered from the immunoprecipitated and input samples was measured by quantitative PCR (qPCR) relative to a standard curve. The qPCR primers used are listed in Extended Data Table 1. Binding was measured as the percentage recovery of immunoprecipitated DNA, relative to the input ($EXP^{REC}$).

To minimize error in the ChIP process, an internal control was built into all experiments. *Xenopus* egg extracts were used to separately replicate a different plasmid, pQUANT (see Extended Data Table 1 for sequences). Mid-way through replication, pQUANT was crosslinked, quenched and spun through Bio-Spin P-6 gel (as above) to yield a single pool of heterologous chromatin that was bound by replication proteins. An equal amount of pQUANT chromatin was added to all experimental chromatin samples before sonication, and this was carried through the entire ChIP procedure. For each set of immunoprecipitations, the recovery of pQUANT ($QNT^{REC}$) should be identical between samples. To correct for technical variation in any set of immunoprecipitations, average pQUANT recovery was calculated ($QNT^{AVG}$) and normalized recovery (%) was calculated as $EXP^{REC}$*$QNT^{AVG}$/$QNT^{REC}$. This ensured that the only sources of technical variation were the crosslinking process and the qPCR. To maximize the reliability of the qPCR, these measurements were performed in quintuplicate and the median value was used. Where three ChIP experiments were combined and plotted as mean ± s.d. (Fig. 5a–c and Extended Data Figs 7f–i and 8j) it was necessary to normalize the data to correct for differences in absolute IP efficiency between experiments. For each protein measured by ChIP, mean recovery across all loci in all samples ($mean^{all}$) was calculated for each experiment ($mean^{all1}$, $mean^{all2}$ and $mean^{all3}$) and used to generate a correction factor for each experiment (for example, for experiment 1 the correction factor is [($mean^{all1}$ + $mean^{all2}$ + $mean^{all3}$)/3]/$mean^{all1}$). To measure dissociation (Fig. 5a–c), recovery of the *FLK2* locus was measured (shown in Extended Data Figs 7f–i and 8j) and peak signal was assigned a value of '0', while background signal (measured at 4 or 5 min for Fig. 5a, or 10 min for Fig. 5b, c) was assigned a value of 100. The experiments shown in Fig. 5a and Extended Data Fig. 7f–i were repeated three times, once with p[*lacO*x12] and twice with p[*lacO*x16].

**Plasmid pull downs.** Plasmid pull downs were performed essentially as described[47], with the following exceptions. Beads were resuspended in buffer supplemented with 4% DMSO and 100 μM NMS-873[48] to block further CMG unloading once the samples were withdrawn[25]. Plasmid-associated proteins from 40–80 ng of plasmid were isolated, and a quarter of the sample was analysed by western blotting using previously described antibodies against CDC45, MCM7 and PCNA[41].

**$HIS_6$-Ub immunoprecipitations.** Ni-NTA Superflow Resin (Qiagen) was washed three times with Urea buffer (10 mM imidazole, 0.2% NP-40, 8 M urea, 500 mM $NaH_2PO_4$, 50 mM Tris HCl, pH 8.0). For each immunoprecipitation, 10 μl of resin was added per tube, and resuspended to 191 μl in Urea buffer. Extracts were supplemented with 100 μM of $HIS_6$-ubiquitin (Boston Biochem) and replication was carried out as described above. At the indicated time, 9 μl of extract was mixed with the bead mix and samples were incubated for 1 h at room temperature, with end-over-end rotation. Resin was washed three times with urea buffer. All residual buffer was removed, and resin was boiled for 5 min in 30 μl sample buffer (125 mM Tris-HCl pH 6.8, 20% glycerol, 6.1% SDS, 0.01% bromophenol blue, 10% β-mercaptoethanol). 30 μl of 0.5 M imidazole was added to each sample and $HIS_6$-tagged proteins were eluted off the resin for 60 min at room temperature, with gentle agitation. Resin was spun down at 1,000 RCF for 1 min, and the supernatant was removed. 10 μl of each sample was resolved on an SDS–PAGE gel alongside an input control and analysed by western blotting using the previously described antibody against MCM7[49]. In Extended Data Fig. 8d, a longer exposure of the IP lanes is shown, since they are far less intense than the input lanes.


45. Prokhorova, T. A., Mowrer, K., Gilbert, C. H. & Walter, J. C. DNA replication of mitotic chromatin in *Xenopus* egg extracts. *Proc. Natl Acad. Sci. USA* **100,** 13241–13246 (2003).
46. Lebofsky, R., Takahashi, T. & Walter, J. C. DNA replication in nucleus-free *Xenopus* egg extracts. *Methods Mol. Biol.* **521,** 229–252 (2009).
47. Budzowska, M., Graham, T. G. W., Sobeck, A., Waga, S. & Walter, J. C. Regulation of the Rev1-pol ζ complex during bypass of a DNA interstrand cross-link. *EMBO J.* **34,** 1971–1985 (2015).
48. Magnaghi, P. *et al.* Covalent and allosteric inhibitors of the ATPase VCP/p97 induce cancer cell death. *Nature Chem. Biol.* **9,** 548–556 (2013).
49. Walter, J. C. & Newport, J. Initiation of eukaryotic DNA replication: origin unwinding and sequential chromatin association of Cdc45, RPA, and DNA polymerase α. *Mol. Cell* **5,** 617–627 (2000).
50. Long, D. T., Räschle, M., Joukov, V. & Walter, J. C. Mechanism of RAD51-dependent DNA interstrand cross-link repair. *Science* **333,** 84–87 (2011).

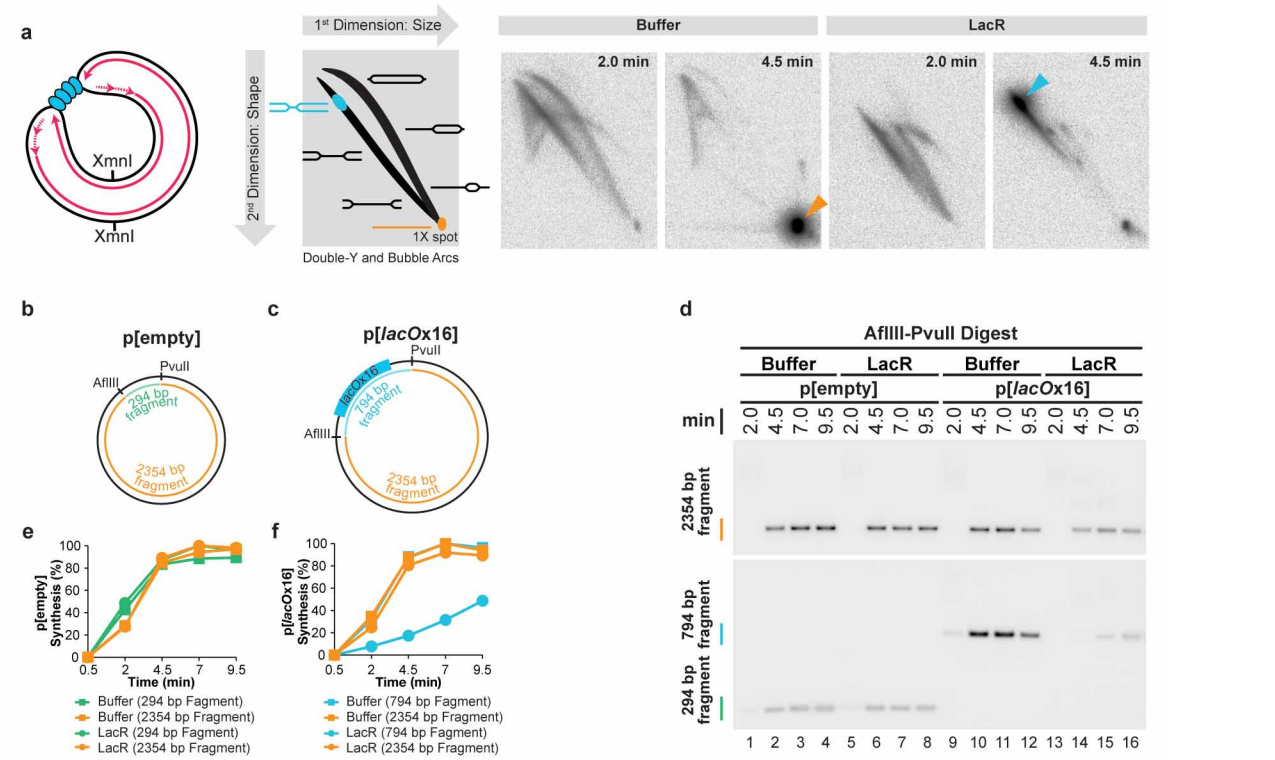


**Extended Data Figure 1 | Sequence-specific termination can be induced at a LacR array.** **a**, To investigate whether a LacR array blocks replication forks, a plasmid containing a tandem array of 16 *lac* operator (*lacO*) sequences, p[$lacO_{16}$] (or p[*lacO*x16]), was incubated with buffer or LacR and then replicated in egg extract containing [$\alpha$-$^{32}$P]dATP. Radiolabelled replication intermediates were cleaved with XmnI (far left cartoon) and separated according to size and shape by 2D gel electrophoresis (see schematic of 2D gel). As replication neared completion at 4.5 min, mainly linear molecules were produced in the presence of buffer (orange arrowhead). In contrast, in the presence of LacR, a discrete spot appeared on the double-Y arc (blue arrowhead), demonstrating that converging replication forks accumulate at a specific locus on p[$lacO_{16}$]. These data indicate that 16 copies of LacR block replication forks. **b**–**f**, To test whether the double-Y structures observed in panel **a** arose from replication forks stalling at the outer edges of the *lacO* array, we tested whether LacR specifically inhibited replication of *lacO* sequences. To this end, p[$lacO_{16}$] (**c**) and the parental plasmid lacking *lacO* repeats, p[empty] (**b**), were incubated in the presence of buffer or LacR and replicated using *Xenopus* egg extracts containing [$\alpha$-$^{32}$P]dATP. Radiolabelled replication intermediates were cleaved with AflIII and PvuII to release the 2,354-bp plasmid backbone (**b** and **c**) and a 294-bp control fragment from p[empty] (**b**) or a 794-bp *lacO* fragment from p[$lacO_{16}$] (**c**). The plasmid backbone and the respective inserts were separated on a native gel and detected by autoradiography (**d**). A longer exposure of the small fragments is shown, since they are less intense than the large fragments. The results in panel **d** were quantified in **e** and **f**. Notably, LacR specifically inhibited replication of the *lacO*-containing fragment in p[$lacO_{16}$] (**f**, blue circles) but not the control fragment in p[empty] (**e**, green circles). We conclude that LacR prevents replication of the *lacO* array and that the double-Ys in panel **a** represent forks converged on the outer edges of the array. Importantly, synthesis within the 2,354-bp backbone fragment (**f**, orange circles) of p[$lacO_{16}$] was not inhibited in the presence of LacR, indicating that no global structural changes occur that inhibit replication.

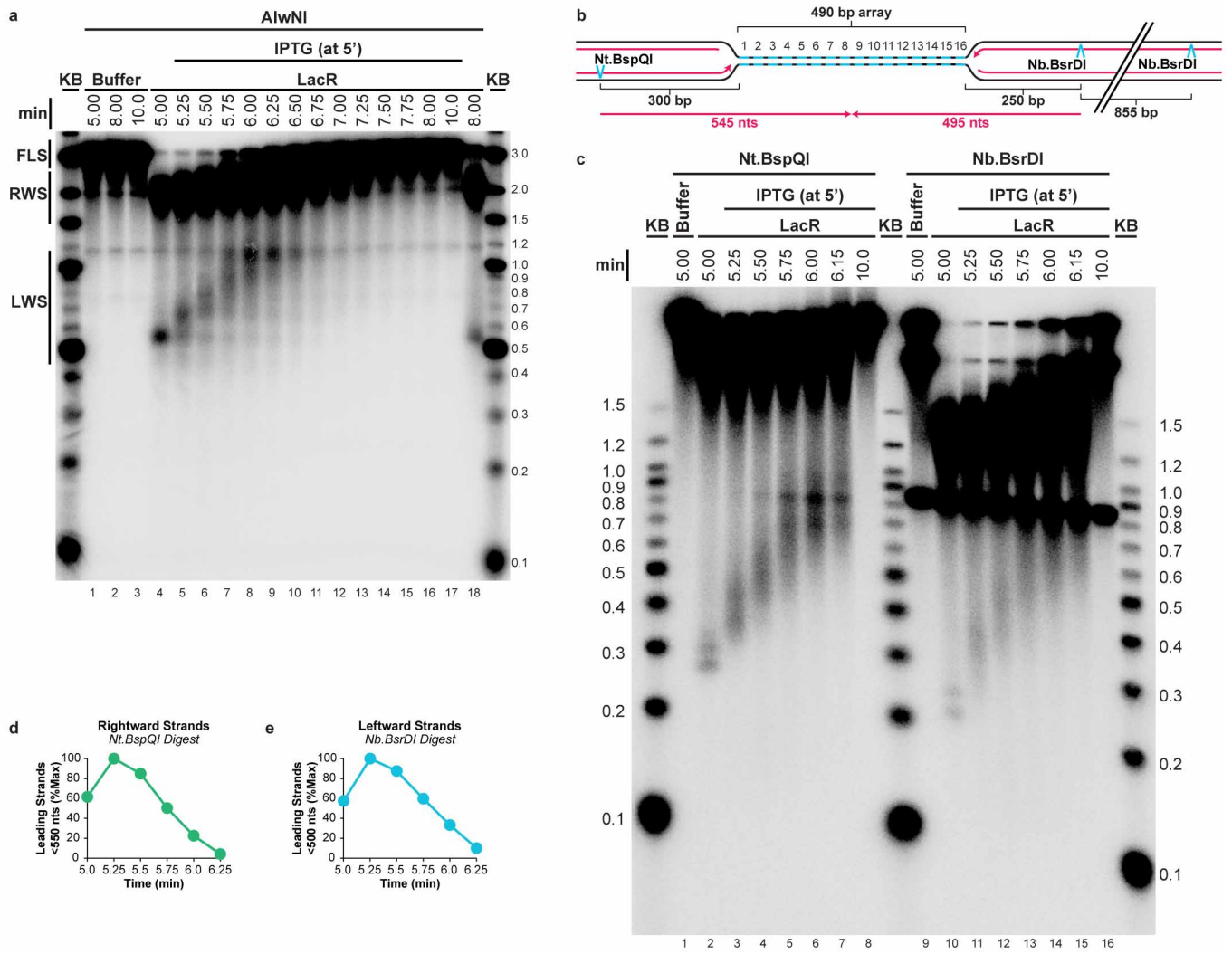


**Extended Data Figure 2 | Supplementary fork progression data.** **a**, The gel shown in Fig. 1e was overexposed and shown in its entirety so that the smaller leftward strands (LWS, Fig. 1d) could be detected. As observed for the rightward strands (RWS, Fig. 1e), LWS rapidly increased in size and then disappeared as they were ligated to produce full-length strands (FLS, Fig. 1e). **b**–**e**, To determine whether the heterogeneity of LWS (**a**) and RWS (Fig. 1e) was due to delayed extension of lagging strands, or because a significant fraction of leading strands did not restart upon IPTG addition, we specifically monitored leading strand progression upon IPTG addition on p[$lacO_{16}$]. To this end, DNA samples were treated with Nt.BspQI or Nb.BsrDI to specifically liberate the rightward or leftward leading strands, respectively (**b**), and DNAs were separated on a denaturing agarose gel (**c**). Before IPTG addition, discrete leading strand products of the expected size were observed (lanes 2 and 10). The presence of two stall products reflects the fact that at a slow rate, the replisome bypasses LacR (see also Fig. 3). Upon IPTG addition, these species rapidly and completely shifted up the gel, indicating that rightward and leftward leading strands restarted efficiently. Therefore, the heterogeneity of the LWS (**a**) and RWS (Fig. 1e) is probably due to delayed ligation of a new Okazaki fragment to the lagging strands. Quantification of leading strands that had not reached the midpoint of the array (rightward and leftward strands smaller than 550 and 500 nt, respectively, **b**) revealed that by 6.25 min, 90% of rightward and leftward leading strands passed the midpoint of the array (**d**, **e**). This demonstrates that leading strands pass each other when forks meet. KB, kilobase ladder, with the length of each band (in kilobases) labelled.

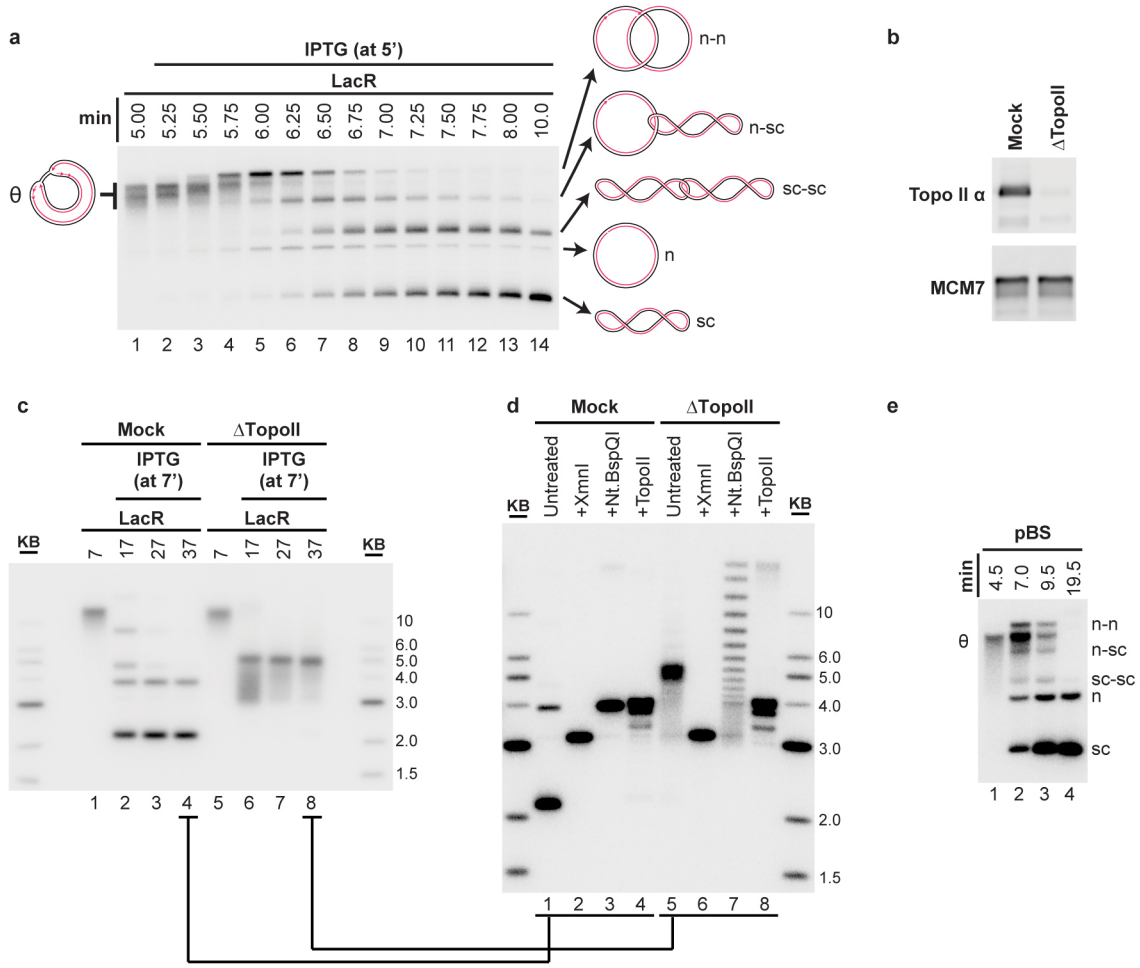


**Extended Data Figure 3 | Topo-II-dependent decatenation of p[lacO$_{16}$].** **a**, The autoradiograph in primary Fig. 1g is reproduced with cartoons indicating the structures of the replication and termination intermediates n–n, n–sc, sc–sc, n and sc (see Fig. 1 for definitions). The order of appearance of the different catenanes matches previous work[5] (n-n, then n-sc, then sc-sc). **b**–**d**, To determine the role of Topo II during termination within a *lacO* array, termination was monitored in mock- or Topo-II-depleted extracts. To confirm immunodepletion of Topo II, mock and Topo-II-depleted NPE was blotted with MCM7 and Topo II antibodies (**b**). p[*lacO*$_{16}$] was incubated with LacR, then replicated in either mock- or Topo-II-depleted egg extracts in the presence of [α-$^{32}$P]dATP, and termination was induced with IPTG (at 7 min). Untreated DNA intermediates were separated by native gel electrophoresis (**c**). In the mock-depleted extract, nicked and supercoiled monomers were readily produced (as in panel **a**, albeit with slower kinetics due to nonspecific inhibition of the extracts by the immunodepletion procedure), while in the Topo-II-depleted extracts, a discrete species was produced. DNA from the last time point in each reaction (lanes 4 and 8 in panel **c**) was purified and treated with XmnI, which cuts p[*lacO*$_{16}$] once, or Nt.BspQI, which nicks p[*lacO*x16] once, or recombinant Topo II, and then separated by native gel electrophoresis (**d**). Cleavage of the mock- and Topo-II-depleted products with XmnI yielded the expected linear 3.15-kb band (lanes 2 and 6), demonstrating that in both extracts all products were fully dissolved topoisomers of each other. Relaxation of the mock-depleted products by nicking with Nt.BspQI yielded a discrete band corresponding to nicked plasmid (lane 3), while the Topo-II-depleted products were converted to a ladder of discrete topoisomers (lane 7), which we infer represent catenated dimers of different linking numbers, since the mobility difference cannot be due to differences in supercoiling. Importantly, the mobility shift after Nt.BspQI treatment (lane 5 versus lane 7) demonstrated that the Topo-II-depleted products (lane 5) were covalently closed and thus in the absence of Topo II, ligation of the daughter strands still occurred. Treatment of the mock- and Topo-II-depleted products with recombinant human Topo II produced the same relaxed monomeric species (lanes 4 and 8), further confirming that the Topo-II-depleted products contained catenanes. Collectively, these observations demonstrate that termination within a *lacO* array in Topo-II-depleted extracts produces highly catenated supercoiled–supercoiled dimers, as seen in cells lacking Topo II[16,17]. These data confirm that Topo II is responsible for decatenation and argue that termination within a *lacO* array reflects physiological termination. **e**, n–n, n–sc, sc–sc, n and sc products were also detected when plasmid lacking *lacO* sequences (pBlueScript) was replicated in the absence of LacR without the use of cyclin A to synchronize replication. Therefore, these intermediates arise in the course of unperturbed DNA replication in *Xenopus* egg extracts.

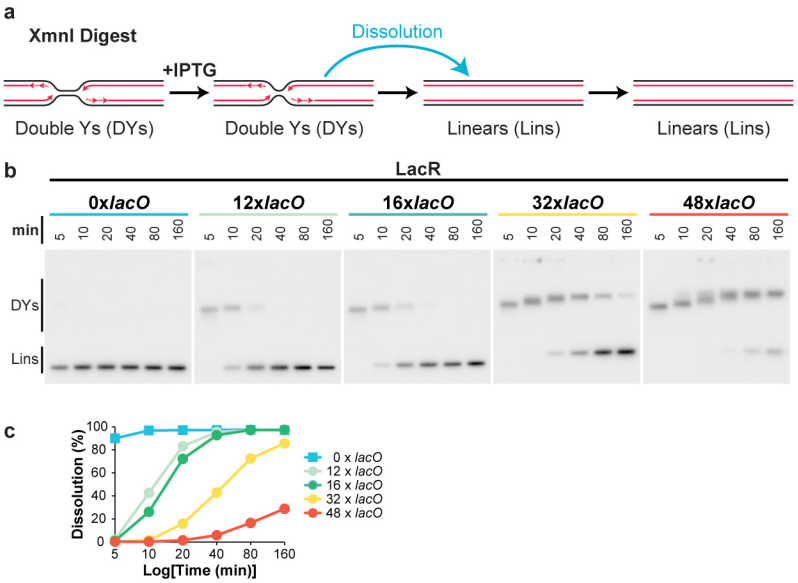


**Extended Data Figure 4 | Inhibition of termination by different-sized LacR arrays.** **a**, Cartoon depicting intermediates detected in the dissolution assay. **b**, To determine the ability of different-sized LacR arrays to inhibit termination, the earliest stage of termination, dissolution (**a**), was monitored in plasmids containing 0, 12, 16, 32, or 48 *lacO* repeats. Plasmids were incubated with LacR, and replicated in the presence of [$\alpha$-$^{32}$P]dATP. To measure dissolution, radiolabelled termination intermediates were cut with XmnI. Cleaved products were separated on a native agarose gel and detected by autoradiography. **c**, Quantification of dissolution in **b**. When 12 or more *lacO* repeats were present in the array, dissolution was robustly inhibited for at least 5 min. Potent inhibition lasted 10 min when 32 *lacO* sequences were present, and 20 min in the presence of 48 *lacO* sequences. In the absence of *lacO* sequences, dissolution was essentially complete by 5 min. Therefore, 12 *lacO* repeats are sufficient to inhibit termination for 5 min.

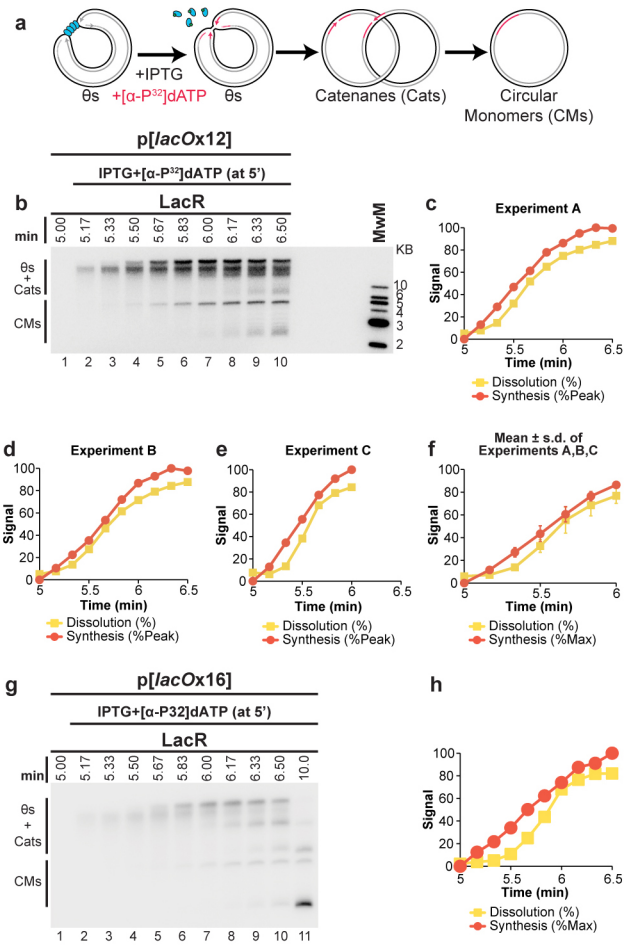


**Extended Data Figure 5 | The rate of total DNA synthesis does not slow before dissolution.** **a**–**c**, To test further whether replication stalls or slows before dissolution, p[$lacO_{12}$] was pre-incubated with LacR and replicated in *Xenopus* egg extracts. Termination was then induced by addition of IPTG after 5 min. Simultaneously, [α-$^{32}$P]dATP was added to specifically radiolabel DNA synthesized after IPTG addition (**a**). Radiolabelled DNA was then separated on a native agarose gel and total signal was measured by autoradiography (**b**). Total signal was quantified, normalized to peak signal, and graphed alongside the rate of dissolution, which was also measured in the same experiment (**c**). This approach gives a highly sensitive measure of DNA synthesis without manipulation of DNA samples. DNA synthesis should occur primarily within the *lacO* array (see Extended Data Fig. 1). Upon IPTG addition, there was an approximately linear increase in signal, which plateaued by 5.83 min. Importantly, dissolution was 65% complete by 5.83 min. Therefore, the large majority of dissolution occurs without stalling of DNA synthesis. **d**, **e**, Experimental repeats of **b**, **c**. **f**, The experiments shown in **c**–**e** were graphed together with mean ± s.d. Synthesis data were normalized so that for each experiment, synthesis at 1 min was assigned a value of 84.4%, since this was the average value from **c**, **d**, where synthesis was allowed to plateau. Given the rate of replication fork progression in these egg extracts (260 bp min$^{-1}$ (ref. 32)) and the size of the array (365 bp), forks should require, on average, 0.7 min to converge if no stalling occurs ((365 bp/2)/260 bp min$^{-1}$ = 0.7 min). The time required for dissolution was not appreciably longer than this (dissolution was 50% complete by 0.67 min after IPTG addition, **f**), consistent with a lack of stalling. **g**, **h**, The experiment shown in **b**, **c** was repeated using p[$lacO_{16}$]. Synthesis was approximately linear until 6.17 min, at which point 81% of molecules had dissolved, further demonstrating that the majority of dissolution occurs without stalling of DNA synthesis.

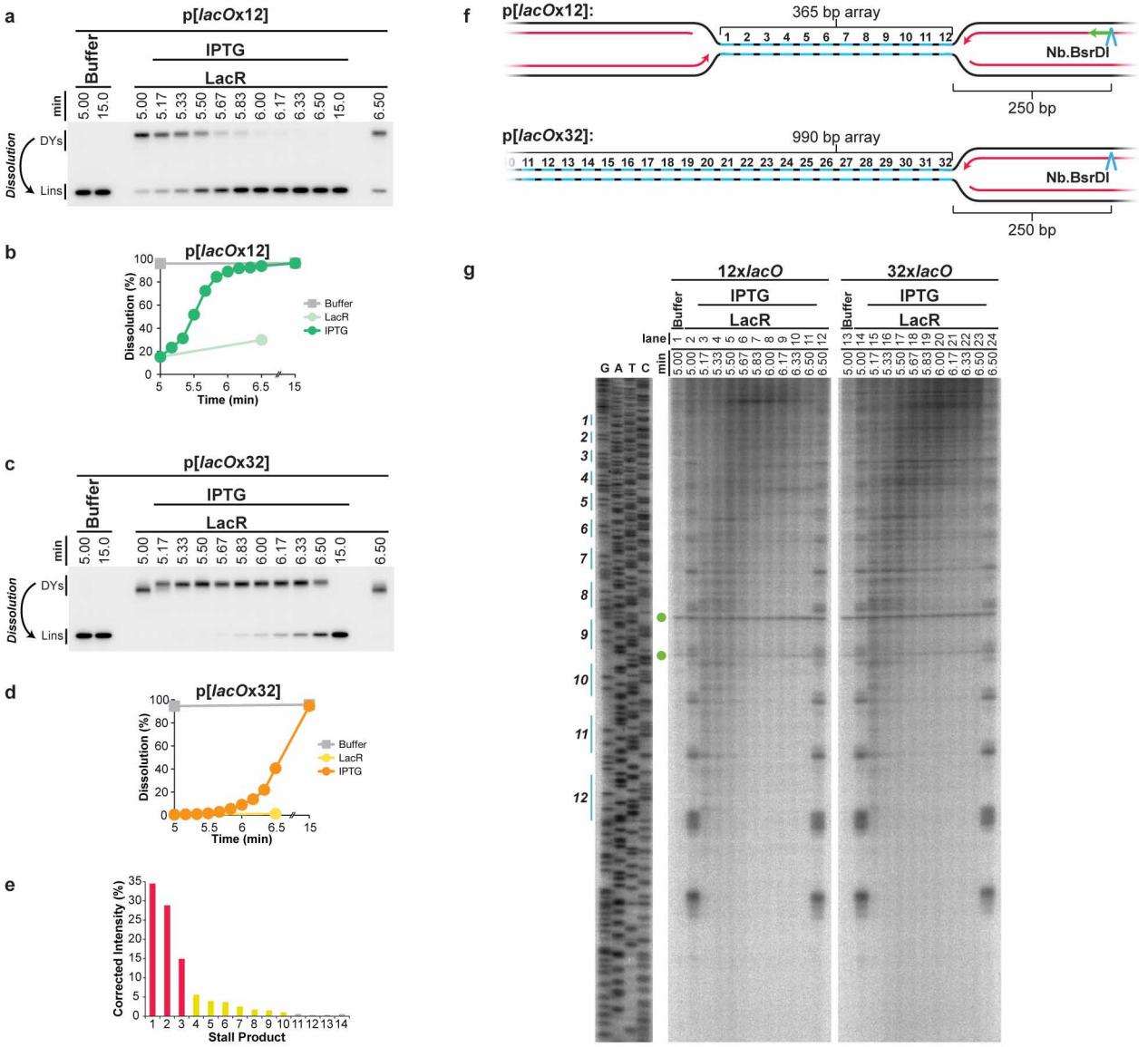


**Extended Data Figure 6 | Replisome progression through 12 and 32 *lacO* arrays.** **a**–**d**, To test whether replisomes meet later in a $lacO_{32}$ array than a $lacO_{12}$ array, we monitored dissolution. LacR block-IPTG release was performed on p[$lacO_{12}$] and p[$lacO_{32}$] and radiolabelled termination intermediates were digested with XmnI to monitor the conversion of double-Y molecules to linear molecules (dissolution). Cleaved molecules were separated on a native agarose gel, detected by autoradiography (**a**, **c**), and quantified (**b**, **d**). Upon IPTG addition, dissolution was delayed by at least 1 min within the 32 *lacO* array compared to the 12 *lacO* array (**b**, **d**). Moreover, by 6 min, 92% of forks had undergone dissolution on p[$lacO_{12}$] while only 9% had dissolved on p[$lacO_{32}$] (**b**, **d**). **e**, Stall products within the 12 *lacO* array (Fig. 3b, lane 2) were quantified, signal was corrected based on size differences of the products, and the percentage of stall products at each stall point was calculated. 78% of leading strands stalled at the first three arrest points (red columns), 19% stalled at the fourth to tenth arrest points (yellow columns) and the remaining 3% stalled at the tenth to fourteenth arrest points (grey columns). The appearance of fourteen arrest points is reproducible but surprising, given that the presence of only 12 *lacO* sequences was confirmed by sequencing in the very preparation of p[$lacO_{12}$] that was used in Fig. 3. The thirteenth and fourteenth arrest points cannot stem from cryptic *lacO* sites beyond the twelfth *lacO* site, as this would position the first leftward leading strand stall product ~90 nucleotides from the *lacO* array, instead of the observed ~30 nucleotides (see **f**, **g**). At present, we do not understand the origin of these stall products. **f**, **g**, Progression of leftward leading strands into the array. The same DNA samples used in Fig. 3 were digested with the nicking enzyme Nb.BsrDI, which released leftward leading strands (**f**), and separated on a denaturing polyacrylamide gel (**g**). The *lacO* sites of p[*lacO*x12] are highlighted in blue on the sequencing ladder (**g**), which was generated using the primer JDO109 (green arrow, **f**). Green circles indicate two nonspecific products of digestion. These products arise because nicking enzyme activity varies between experiments, even under the same conditions. There was no significant difference in the pattern of leftward leading strand progression between the 12 *lacO* and 32 *lacO* arrays, as seen for the rightward leading strands (Fig. 3b). Specifically, by 5.67 min, the majority of leading strands had extended beyond the seventh *lacO* repeat within $lacO_{12}$ (lane 6) and the equivalent region of $lacO_{32}$ (lane 18). Therefore, progression of leftward leading strands is unaffected by the presence of an opposing replisome, suggesting that converging replisomes do not stall when they meet.

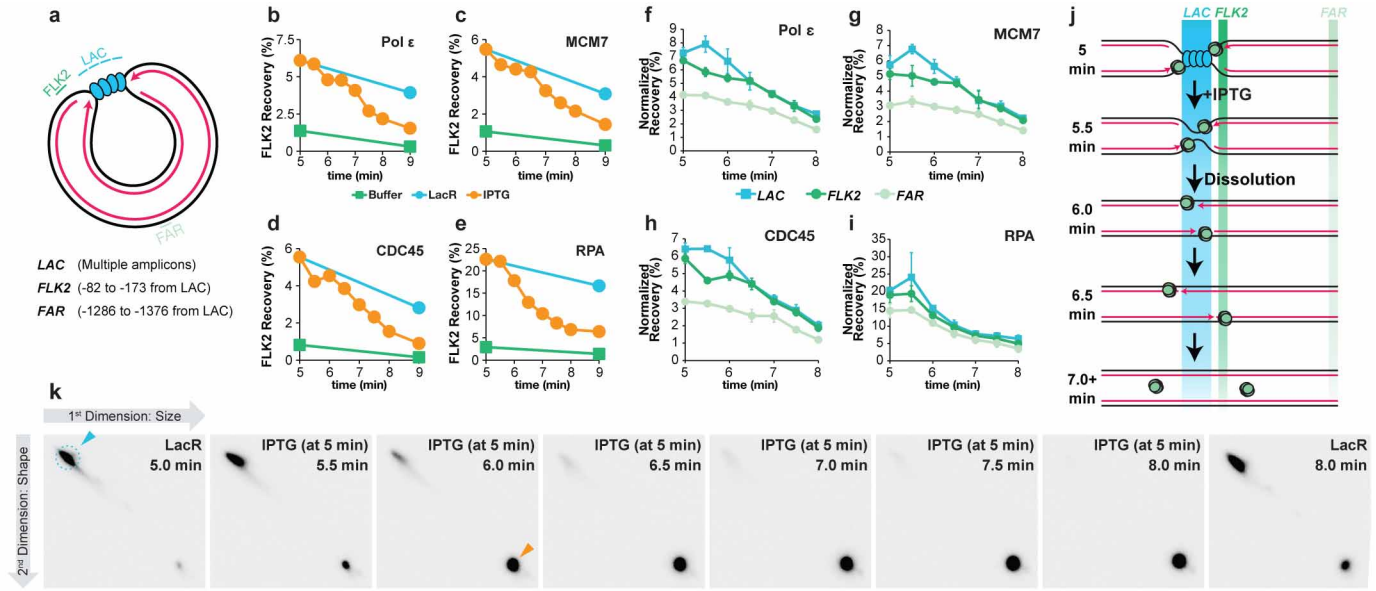


**Extended Data Figure 7 | Supplementary ChIP data.** **a**, Cartoon depicting the *LAC*, *FLK2* and *FAR* loci, which were used for ChIP. Their precise locations relative to the leftward edge of the *lacO* array are indicated. The *LAC* amplicon is present in four copies distributed across the $lacO_{16}$ array and three copies distributed across the $lacO_{12}$ array. **b**–**e**, p[*lacO*x12] was incubated with buffer or LacR and termination was induced at 5 min by IPTG addition. MCM7, RPA, CDC45 and Polε ChIP was performed at different time points after IPTG addition but also in the buffer control and no IPTG control. Recovery of *FLK2* was measured as a percentage of input DNA. Upon IPTG addition, ChIP signal declined and by 9 min was comparable to the buffer control, demonstrating that unloading of replisomes was induced within 4 min of IPTG addition. **f**, To test whether movement of the replisome into and out of the *lacO* array could be detected upon IPTG addition, termination was monitored within a *lacO* array, and we performed ChIP of the leading strand polymerase Polε, which was inferred to move into and out of the array based on the behaviour of leading strands during termination (Extended Data Fig. 2b–e). It was predicted that Polε ChIP at the *LAC* locus should increase slightly as Polε enters the *lacO* array and decline again as converging polymerases pass each other, but persist at *FLK2* while the polymerases move out of the array. Before IPTG addition, Polε was enriched at *LAC* and *FLK2* compared to *FAR*, consistent with the leading strands being positioned on either side of the *lacO* array (Extended Data Fig. 2c and Fig. 3). Upon IPTG addition, Polε became modestly enriched at *LAC* compared to *FLK2* (5.5 min) but then declined to similar levels at both *LAC* and *FLK2* by 6.5 min. These data are consistent with the leading strand polymerases entering the *lacO* array and passing each other. **g**, **h**, To test whether CMG exhibited the same ChIP profile as Polε, MCM7 and CDC45 ChIP was performed using the same samples. After IPTG addition, MCM7 and CDC45 were enriched at *LAC* compared to *FLK2* (5.5 min), then declined to similar levels at both *LAC* and *FLK2* by 6.5 min, as seen for Polε (**f**). These data are consistent with a model in which CMGs enter the array and pass each other during termination. A caveat of these experiments is the relatively high recovery of the *FAR* locus in MCM7, CDC45 and Polε ChIP. Specifically, signal was at most only ~2-fold enriched at *LAC* compared to *FAR*. This was not due to high background binding, because by the end of the experiment (10 min time point, not shown) we observed a decrease in signal of ~5–7-fold. Furthermore, we observed ~5–7-fold enrichment in binding (ChIP) of replisome components to p[$lacO_{12}$] that had been incubated in LacR compared to a buffer control (see **g**–**i**, below). Instead, the high *FAR* signal was probably due to poor spatial resolution of the ChIP. Consistent with this, when a plasmid containing a DNA interstrand cross-link (ICL) was replicated, essentially all replisomes converged upon the ICL but the ChIP signal for MCM7 and CDC45 was only ~3–4-fold enriched at the ICL compared to a control locus[41]. We speculate that the higher background observed at the control locus in our experiments is due to the decreased distance of the control locus from the experimental locus (1.3 kb for p[$lacO_{16}$] and p[$lacO_{12}$] versus 2.4 kb for the ICL plasmid) and possibly due to increased catenation of the parental strands during termination. The high signal at *FAR* should not complicate interpretation of the MCM7, CDC45 and Polε ChIP (**f**), as signal at *FAR* was essentially unaltered between 5 and 6.5 min. Further evidence that the high signal seen at the *FAR* locus emanates from forks stalled near the *lacO* array is presented in panel **k**. **i**, ChIP of RPA was performed on the same chromatin samples used in **b**–**d**. As seen for Polε, MCM7 and CDC45, enrichment of RPA at *LAC* compared to *FAR* was relatively low, consistent with poor spatial resolution. **j**, Predicted binding of CMGs to the *LAC*, *FLK2* and *FAR* loci before and after IPTG addition if converging CMG pass each other. **k**, To determine whether most forks stalled at the array and not elsewhere in the plasmid, we performed a time course in which p[$lacO_{16}$] undergoing termination was examined by 2D gel electrophoresis at various time points. p[$lacO_{16}$] was pre-bound to LacR and replicated in *Xenopus* egg extract containing [$\alpha$-$^{32}$P]dATP. Termination was induced by IPTG addition and samples were withdrawn at different times. Radiolabelled replication intermediates were cleaved with XmnI (as in Extended Data Fig. 1a) and separated according to size and shape on 2D gels[50]. A parallel reaction was performed in which samples were analysed by ChIP, which was one of the repeats analysed in **b**–**e**. In the presence of LacR, a subset of double-Y molecules accumulated (blue arrowhead), demonstrating that 83% of replication intermediates (signal in dashed blue circle) contained two forks converged at a specific locus. After IPTG addition, linear molecules rapidly accumulated (orange arrowhead) as dissolution occurred. Importantly, the vast majority of signal was present in the discrete double-Y and linear species (blue and orange arrowheads), demonstrating that the relatively high ChIP signal observed at *FAR* in panels **f**–**i** was derived from forks present at the $lacO_{16}$ array and not elsewhere.

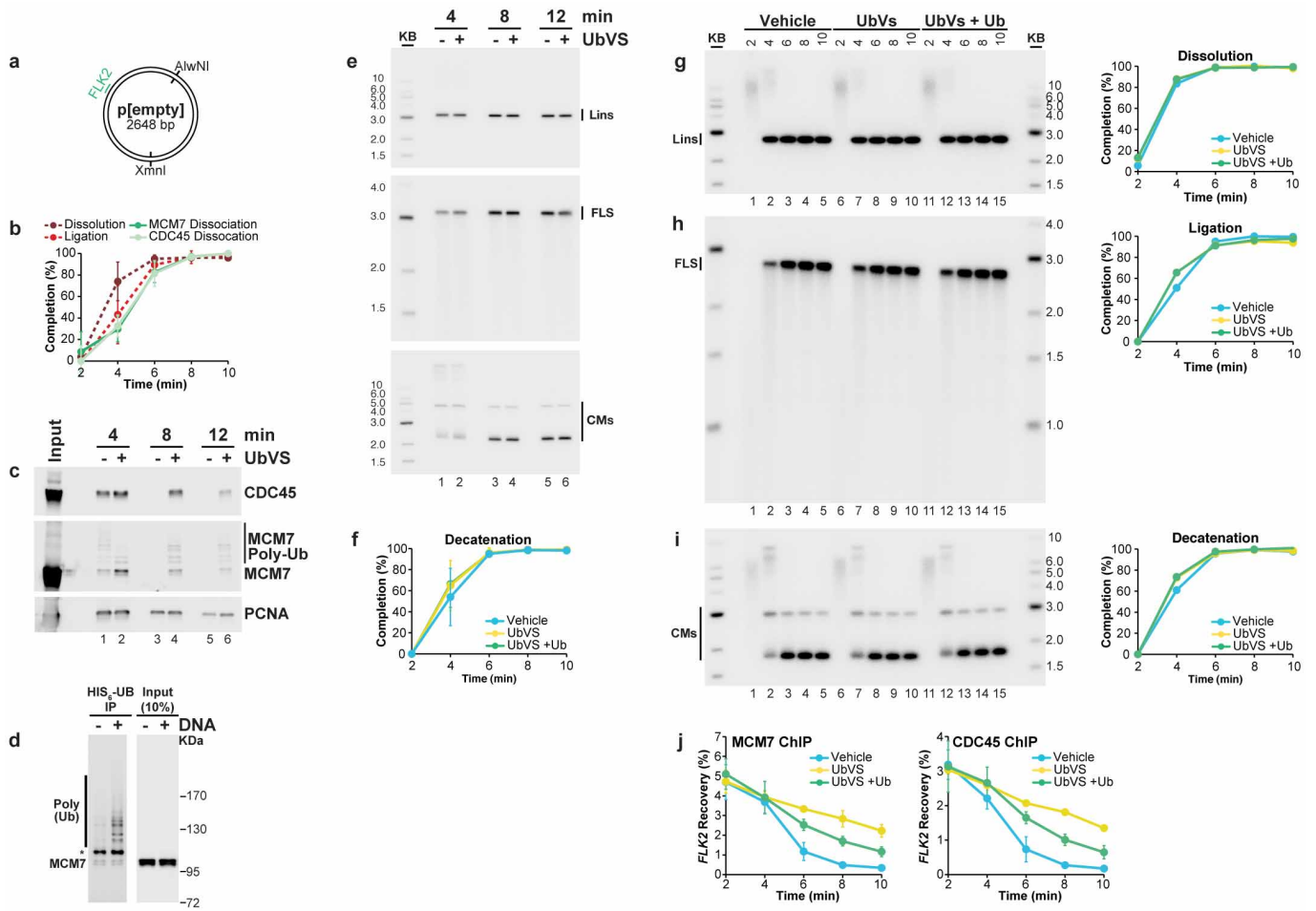


**Extended Data Figure 8 | Supplementary termination data for p[empty] experiments.** **a**, Cartoon depicting the XmnI and AlwNI sites on p[empty], which are used for the dissolution and ligation assays, respectively, and the *FLK2* locus, which is used for ChIP. **b**, Plasmid DNA without a *lacO* array (p[empty]) was replicated and at different times chromatin was subjected to MCM7 and CDC45 ChIP. Per cent recovery of *FLK2* was quantified and used to measure dissociation of MCM7 and CDC45 (see Methods). Dissolution and ligation were also quantified in parallel. Mean ± s.d. is plotted ($n = 3$). The MCM7 and CDC45 dissociation data are obtained from the vehicle controls in Fig. 5b, c, while the dissolution and ligation data are obtained from the vehicle controls in Fig. 5d, e. **c**, To seek independent evidence for the conclusions of the ChIP data presented in Fig. 5b, c, we used a plasmid pull-down procedure. p[empty] was replicated in egg extracts treated with vehicle or Ub-VS. At the indicated times, chromatin-associated proteins were captured on LacR-coated beads (which binds DNA independently of *lacO* sites) and analysed by western blotting for CDC45, MCM7 and PCNA. CDC45 and MCM7 dissociated from chromatin by 8 min in the vehicle control, but persisted following Ub-VS treatment. **d**, To test whether the MCM7 modifications detected in panel **c** represented ubiquitylation, extracts were incubated with $His_6$-ubiquitin in the absence of cyclin A, and in the absence or presence of plasmid DNA. After 15 min, $His_6$-tagged proteins were captured by nickel resin pull down and blotted for MCM7. DNA replication greatly increased the levels of ubiquitylated MCM7, with the exception of a single species that was ubiquitylated independently of DNA replication (*). These data show that MCM7 is ubiquitylated during plasmid replication in egg extracts, as observed in yeast and during replication of sperm chromatin after nuclear assembly in egg extracts[24,25]. **e**, In parallel to the plasmid pull downs performed in **c**, DNA samples were withdrawn for dissolution, ligation and decatenation assays, none of which was perturbed by Ub-VS treatment. These data support our conclusion, based on ChIP experiments (Fig. 5), that defective CMG unloading does not affect dissolution, ligation, or decatenation. **f**, Decatenation was measured in the same reactions used to measure dissolution and ligation (Fig. 5d, e), mean ± s.d. is plotted ($n = 3$). **g**–**i**, Given the experimental variability at the 4 min time point in Fig. 5d–f, the primary data and quantification for dissolution (**g**), ligation (**h**) and decatenation (**i**) for one of the three experiments summarized in Fig. 5d–f is presented. This reveals that Ub-VS does not inhibit dissolution, ligation, or decatenation at the 4 min time point. The same conclusion applies to two additional repetitions of this experiment (data not shown). **j**, The primary ChIP data used to measure dissociation of MCM7 and CDC45 in Fig. 5b, c is shown. Recovery of *FLK2* was measured. Mean ± s.d. is plotted ($n = 3$).

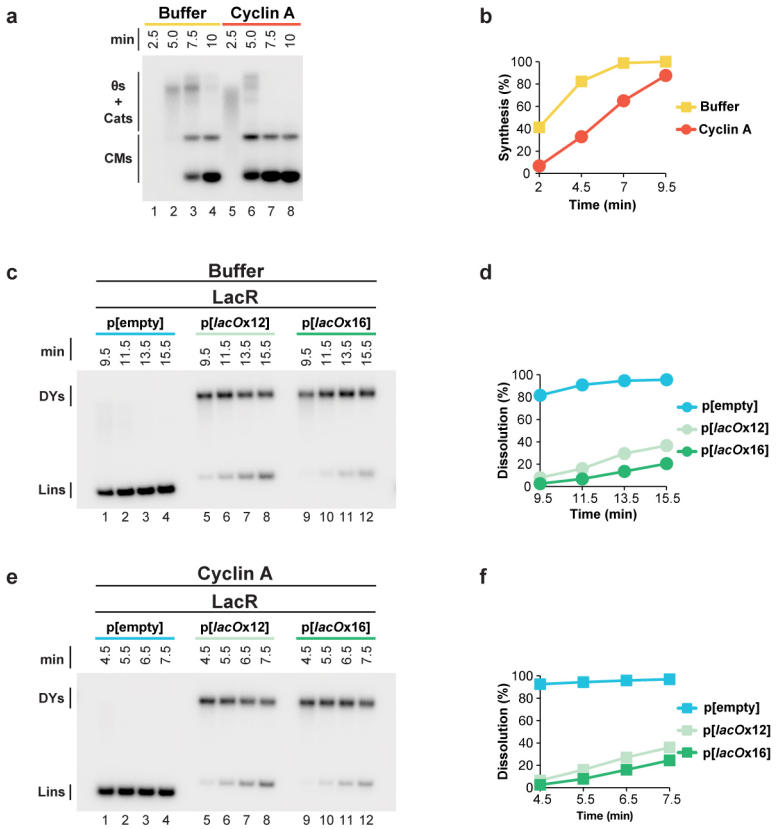


**Extended Data Figure 9 | Cyclin A treatment synchronizes DNA replication in *Xenopus* egg extracts.** **a**, **b**, To synchronize DNA replication in *Xenopus* egg extracts, we treated extracts with cyclin A, which probably accelerates replication initiation[45]. Plasmid DNA was incubated in High Speed Supernatant for 20 min, then either buffer or cyclin A was added for a further 20 min. NucleoPlasmic extract was added to initiate DNA replication, along with [α-$^{32}$P]dATP to label replication intermediates. Replication products were separated on a native agarose gel, detected by autoradiography (**a**), and quantified (**b**). In the presence of vehicle, replication was not complete by 9.5 min, but in the presence of cyclin A, replication was almost complete by 4.5 min (**b**). Thus, cyclin A treatment approximately doubles the speed of DNA replication in *Xenopus* egg extracts. **c**–**f**, To test whether cyclin A affects the ability of LacR to inhibit termination, we monitored dissolution of plasmids containing a 12 or 16 LacR array in the presence and absence of cyclin A. p[$lacO_{12}$], p[$lacO_{16}$], and the parental control plasmid p[empty] were incubated with LacR, and then treated with buffer or cyclin A before replication was initiated with NPE in the presence of [α-$^{32}$P]dATP. Samples were withdrawn when dissolution of p[empty] plateaued (9.5 min in the presence of buffer, 4.5 min in the presence of cyclin A). Given that cyclin A treatment approximately doubles the speed of replication (see **b**), samples were withdrawn from these reactions twice as frequently as the buffer-treated samples. To measure dissolution, radiolabelled termination intermediates were cut with XmnI to monitor the conversion of double-Y molecules to linear molecules. Cut molecules were separated on a native agarose gel and detected by autoradiography (**c**, **e**). By the time the first sample was withdrawn, dissolution of p[empty] was essentially complete, in the absence (9.5 min, **d**) or presence (4.5 min, **f**) of cyclin A. Importantly, dissolution of p[$lacO_{12}$] and p[$lacO_{16}$] was prevented in the absence (9.5 min, **d**) or presence (4.5 min, **f**) of cyclin A. Moreover, dissolution occurred approximately twice as fast in the presence of cyclin A (note the similarity between **d** and **f** even though samples are withdrawn twice as frequently in **f**) consistent with replication being approximately twice as fast in the presence of cyclin A. Therefore, cyclin A does not affect the ability of a LacR array to block replication forks.

**Extended Data Table 1 | Tables of plasmids and oligonucleotides used**

**A.**

| Plasmid | Insert | Construction |
|---|---|---|
| pJD82 | SacI-BsrGI-(lacO)x4-BsiWI-KpnI | Replacement of the sequence between SacI and KpnI of pBluescript II KS- |
| pJD85 | SacI-BsrGI-(lacO)x8-BsiWI-KpnI | JDO38/39 annealed and cloned into pJD82 that had been cut with BsrGI |
| pJD88 | SacI-BsrGI-(lacO)x16-BsiWI-KpnI | BsrGI/BsiWI fragment from pJD85 cloned into pJD85 that had been cut with BsrGI |
| pJD92 | SacI-BsrGI-(lacO)x32-BsiWI-KpnI | BsrGI/BsiWI fragment from pJD88 cloned into pJD88 that had been cut with BsrGI |
| pJD100 | SacI-BsrGI-(lacO)x48-BsiWI-KpnI | BsrGI/BsiWI fragment from pJD88 cloned into pJD92 that had been cut with BsrGI |
| pJD104 | SacI-BsrGI-(lacO)x12-BsiWI-KpnI | JDO38/39 annealed and cloned into pJD85 that had been cut with BsrGI |
| pJD105 | SacI-Nb.BsmI-BsiWI-Nt.BbvCI-KpnI | Replacement of the sequence between SacI and KpnI of pBluescript II KS- with JDO42/43 |
| pJD139 | SacI-Nb.BsmI-BsiWI-Nt.BbvCI-KpnI | Quickchange mutagenesis of pJD105 using JDO94/95 |
| pJD145 | SacI-Nb.BsmI-BsiWI-Nt.BbvCI-KpnI | Quickchange mutagenesis of pJD139 using JDO100/10 |
| pJD150 | SacI-Nb.BsmI-(lacO)x12-BsiWI-Nt.BbvCI-KpnI | BsrGI/BsiWI fragment from pJD104 cloned into pJD145 that had been cut with BsiWI |
| pJD152 | SacI-Nb.BsmI-(lacO)x16-BsiWI-Nt.BbvCI-KpnI | BsrGI/BsiWI fragment from pJD88 cloned into pJD145 that had been cut with BsiWI |
| pJD156 | SacI-Nb.BsmI-(lacO)x32-BsiWI-Nt.BbvCI-KpnI | BsrGI/BsiWI fragment from pJD92 cloned into pJD145 that had been cut with BsiWI |
| pQNT | - | pCDFDuet-1 containing a HincII site (pQuant from [41]) |

**B.**

| Oligo | Sequence | Description |
|---|---|---|
| JDO38 | 5′-GTACATCAATTGTGAGCGGATAACAATTGTTAGGGAGGAATTGTGAGCGGATAACAATTTGGAGTTGATAATTGTGAGCGGATAACAATTGGCTTCAACGTAATTGTGAGCGGATAACAATTTCC-3′ | Can be annealed to JDO39 to generate dsDNA containing 4x lacO sites with ends that are compatible with BsiWI and BsrGI. |
| JDO39 | 5′-GTACGGAAATTGTTATCCGCTCACAATTACGTTGAAGCCAATTGTTATCCGCTCACAATTATCAACTCCAAATTGTTATCCGCTCACAATTCCTCCCTAACAATTGTTATCCGCTCACAATTGAT-3′ | Can be annealed to JDO38 to generate dsDNA containing 4x lacO sites with ends that are compatible with BsiWI and BsrGI. |
| JDO42 | 5′-CTGTACAGCATTCCCATGGCGTACGTTCTAGACCTCAGCTATGGTACC-3′ | Can be annealed to JDO43 to generate dsDNA containing sites for BsrGI-Nb.BsmI-NcoI-BsiWI-XbaI-Nb.BbvCI with ends that are compatible with SacI and KpnI. |
| JDO43 | 5′-AGCGGTACCATAGCTGAGGTCTAGAACGTACGCCATGGGAATGCTGTACAGAGCT-3′ | Can be annealed to JDO42 to generate dsDNA containing sites for BsrGI-Nb.BsmI-NcoI-BsiWI-XbaI-Nb.BbvCI with ends that are compatible with SacI and KpnI. |
| JDO94 | 5′-TAAGGGATTTTGCCGATTTCGGCCTATGCTCTTCGCAGTGTGGTTAAAAAATGAGC-3′ | Used with JDO95 to introduce Nt.BspQI and Nb.BtsI sites upstream of Nb.BsmI in pJD105-derived plasmids by Quickchange mutagenesis. |
| JDO95 | 5′-GCTCATTTTTTAACCACACTGCGAAGAGCATAGGCCGAAATCGGCAAAATCCCTTA-3′ | Used with JDO94 to introduce Nt.BspQI and Nb.BtsI sites upstream of Nb.BsmI in pJD105-derived plasmids by Quickchange mutagenesis. |
| JDO100 | 5′-TGAGCGTCGATTCATTGCTTTGTGATGCTCGTCAGGGGG-3′ | Used with JDO101 to introduce Nb.BsrDI site downstream of BbvCI in pJD105-derived plasmids by Quickchange mutagenesis. |
| JDO101 | 5′-CCCCCTGACGAGCATCACAAAGCAATGAATCGACGCTCA-3′ | Used with JDO100 to introduce Nb.BsrDI site downstream of BbvCI in pJD105-derived plasmids by Quickchange mutagenesis. |
| JDO107 | 5′-CAGTGTGGTTAAAAAATGAGCTG-3′ | Sequencing primer for mapping leading strands released by Nt.BspQI digestion |
| JDO109 | 5′-CATTGCTTTGTGATGCTCGT-3′ | Sequencing primer for mapping leading strands released by Nb.BsrDI digestion |
| JDO110 | 5′-TGGTTAAAAAATGAGCTGATTTAACA-3′ | Sequencing primer for mapping lagging strands released Nb.BtsI digestion. |
| JDO111 | 5′-TGAGGTCTAGAACGTACGGAAA-3′ | Sequencing primer for mapping leading strands released by Nb.BbvCI digestion. |
| FLK2_F | 5′-TCTTCGCTATTACGCCAGCT-3′ | Used with FLK2_R to amplify the region 82-173 bases upstream of the lacO array in pJD152 |
| FLK2_R | 5′-TTACAACGTCGTGACTGGGA-3′ | Used with FLK2_F to amplify the region 82-173 bases upstream of the lacO array in pJD152 |
| LAC_F | 5′-AGCGGATAACAATTGTTAGGGA-3′ | Used with LAC_R to amplify four sites within the lacO array in pJD152 |
| LAC_R | 5′-CTCACAATTACGTTGAAGCCAA-3′ | Used with LAC_F to amplify four sites within the lacO array in pJD152 |
| FAR_F | 5′-ATTGCTACAGGCATCGTGGT-3′ | Used with FAR_R to amplify the region 1286-1375 bases upstream of the lacO array in pJD152 |
| FAR_R | 5′-GGGATCATGTAACTCGCCTTGA-3′ | Used with FAR_F to amplify the region 1286-1375 bases upstream of the lacO array in pJD152 |
| QNT_F | 5′-TACAAATGTACGGCCAGCAA-3′ | Used with QNT_R to amplify pQNT |
| QNT_R | 5′-GAGTATGAGGGAAGCGGTGA-3′ | Used with QNT_F to amplify pQNT |